Influence of types of binder and plant aggregates on hygrothermal and mechanical properties of vegetal concretes

Méryl Lagouin, Camille Magniont, Pascale Senechal, Peter Moonen, Jean-Emmanuel Aubert, Aurélie Laborel-Préneron

Influence of types of binder and plant aggregates on hygrothermal and mechanical properties of vegetal concretes

Méryl LAGOUIN[1], Camille MAGNIONT[1], Pascale SENECHAL[2], Peter MOONEN[2,3], Jean-Emmanuel AUBERT[1],
Aurélie LABOREL-PRÉNERON[1]

[1] *LMDC, Université de Toulouse, INSA, UPS, France*
[2] CNRS/ Univ Pau & Pays Adour/ E2S UPPA, DMEX-IPRA, UMS3360, France
[3] CNRS/ Total/ Univ Pau & Pays Adour/ E2S UPPA, LFCR-IPRA, UMR5150, France

ABSTRACT. Bio-aggregate based building materials offer promising perspectives thanks to their low environmental impact and interesting hygrothermal behaviour. In this paper, different formulations of bio-aggregate concrete are proposed and analysed. We focus on two types of locally available bio-aggregates, namely maize and sunflower bark chips, and two types of binder matrices, based on respectively metakaolin and lime. The study specifically focuses on the pore structure of the composite material, as this quantity has a decisive impact on the insulating properties (thermal conductivity), the hygric behaviour (sorption isotherms, water vapour permeability and moisture buffer value) as well as on the mechanical performance (compressive strength). The results underline the impact of the constituents' porosity on the complex porous structure of the bio-concrete and the influence of porosity on its performance. The findings demonstrate that metakaolin and sunflower are high-potential raw materials for the design of a bio-aggregate based concrete.

KEYWORDS: bio-based materials; porosity; X-ray tomography; sorption isotherm; water vapour permeability; moisture buffer value; thermal conductivity; compressive strength

1 INTRODUCTION

Growing ecological and environmental awareness has driven efforts from all sectors to reduce their global environmental footprint. The building industry is particularly concerned since buildings are responsible for approximately 40 % of energy consumption and 36 % of greenhouse gas emissions in the European Union (European Commission, 2018). This sector is the largest consumer of energy and non-renewable raw materials and the largest producer of waste in France (ADEME, 2018; Ghewy, 2017; SOeS, 2016). Consumption of resources, such as energy and raw materials, as well as greenhouse gas and pollutant emissions underlie the main impacts of buildings on the environment.

These observations have contributed to the rapid expansion of innovative and sustainable materials. Plant-based building materials are some of them. They are obtained from the processing of agricultural by-products, such as hemp, and have considerable environmental benefits. First, bio-aggregates are derived from an abundant, renewable vegetal resource which is also a carbon sequestration material as agricultural products have the property of capturing carbon dioxide from the atmosphere during their growth and storing it in their organisms. Besides, the use of plant particles in building materials helps to economize valuable natural resources thanks to agricultural waste recovery (Peñaloza et al., 2016).

Associated with a mineral binder to bind the particles together, plant aggregates enable the design of bio-aggregate-based concrete. These lightweight vegetal concretes are hygroscopic materials. Thus, they have the capacity to store moisture from or release it into the ambient air and, hence, to moderate daily or seasonal humidity variations and sudden step changes of the indoor environment (Moujalled et al., 2018). Their low thermal conductivity enables them to reduce heat diffusion, and thus winter heat losses, and protect from summer heat waves (Tran Le et al., 2010). Thanks to their ability to manage water vapour transfer and to regulate heat flows, vegetal concretes ensure high indoor environmental quality and contribute to energy saving (Amziane and Collet, 2017), while limiting the environmental impacts of building materials.

Hemp concrete has been the most commonly investigated bio-aggregate based material in recent years. However, hemp is not widely produced in France and little is available in the south-west of the country. To minimize transport distances and thus lower carbon emissions, the raw material has to be locally available. Hence, it appeared necessary to seek other potential agricultural by-products, produced in greater quantities. The potential of several agricultural wastes has been studied, such as sunflower stem (Nozahic, 2012), lavender stalk (Ratiarisoa et al., 2016), barley straw and corn cob (Laborel-Préneron et al., 2017), flax, rape, corn and wheat (Viel et al., 2018).

Some authors have explored the complex porous structure of bio-composites, mostly of hemp concrete. With a total porosity ranging from 60 to 80 %, these materials are defined as highly porous (Cérézo, 2005; Chamoin, 2013; Collet et al., 2008, 2013; Driss; Evrard, 2008; Glé et al., 2011; Gourlay et al., 2017; Rahim et al., 2016). The pore shape and connection structure (open and closed) depend on the formulation and manufacturing methods, among other things. This can partly explain the variability of porosity values. The open porosity value, close to the total porosity, reflects the high interconnection of the wide range of pore sizes (Cérézo, 2005; Chamoin, 2013; Collet et al., 2008, 2013).

The (open) pore size distribution of hemp concrete seems to be tri-modal (Cérézo, 2005; Chamoin, 2013; Collet et al., 2008, 2013; Dubois, 2014; Evrard, 2008; Glé et al., 2011; Lawrence et al., 2012) and comprises the intra-binder microporosity (about 1 µm width), the mesoscopic porosity of hemp shives (around 10 µm) and the macroscopic porosity between shives in the binder (> 1 mm).

Despite its straightforward definition, porosity cannot be easily quantified since the pore sizes span a wide range (from a few nanometers to millimeters or larger). There is no single technique that adequately covers this wide range of scales, which might explain the huge variability of porosity values found in literature for vegetal concrete. Image analysis, physisorption, gas pycnometry and mercury porosimetry are commonly used methods but all have limitations, such as the detection threshold. In addition, the porosity can be modified or changed by a variety of processes during its measurement. These include deformation, hydrothermal alteration and the production of secondary or fracture porosity (Amziane and Collet, 2017).

The high porosity and the microstructure of bio-aggregates are fundamental to their physical properties. Typically, they have a low density and a complex pore structure. This has two main consequences. First, low density is associated with low strength, but also with low thermal conductivity. Secondly, the complex nature of the porosity results in a material that is able to adsorb moisture and humidity readily. It thus has an exceptionally high moisture buffering capacity (Collet et al., 2013; Evrard, 2008; Latif et al., 2015; Palumbo et al., 2016; Ratiarisoa et al., 2016; Tran Le et al., 2010), a characteristic that is of great interest for building materials because it tends to stabilize the internal environment of a building, thereby resulting in much healthier indoor conditions.

The open and interconnected pores are also places where heat and mass transfer and moisture storage take place. From a hygric point of view, varying the composition (nature of binder and aggregates) can modify the capacity of concretes to hold water in their capillaries, especially at the highest humidities, where capillary condensation occurs (Chamoin, 2013; Collet et al., 2013; Rahim et al., 2015, 2016; Walker and Pavía, 2014). Chamoin, (2013) and Collet et al., (2013) state that capillary condensation is found in the skin of the cell walls of particles and in the inter-particular pores of the binder (pores of width from 0.005 to 0.040 µm). It is shown by Rahim et al. (2015, 2016) that the sorption isotherm patterns of vegetal concretes with different types of bio-aggregates are similar for low and medium hygrometry (due to the similar microstructure). For a relative humidity higher than 80 %, the smaller pore size in rape straw and flax shives (compared to hemp) promotes capillary condensation. It results in higher moisture adsorption values: 160 kg/m³ of moisture content compared to 95 kg/m³ for hemp lime concrete at 95 % RH. Furthermore, the effect of the type of binder on the capillary action of hemp concrete is demonstrated. In particular, according to Walker and Pavía (2014), referring to Evrard (2003) as well as their own results, increasing the hydraulicity of the binder reduces capillary absorption. As reported by these authors, it is likely that hydrates reduce capillary action by filling pores. This is similar to the behaviour of cement-lime pastes: the porosity decreases greatly with increasing amounts of cement in the paste while the complexity of the microstructure increases. Thus, the capillary coefficient drops with increasing cement content due to the hydration (Arandigoyen and Alvarez, 2006).

In addition, the type of bio-aggregate affects the water vapour permeability. According to Rahim et al., (2015, 2016), the water vapour permeability of hemp concrete is evaluated as being slightly smaller than that of flax and rape straw concretes. Ratiarisoa et al. (2016) reveal the lower vapour resistance of composites made with lavender stalks in comparison with other bio-aggregate based building materials (straw-clay, wood and hemp concretes) that have lower densities. Such results could be linked with the morphology of the particles. The long, elongated, porous particles could facilitate water vapour transfer through the specimen in comparison with rounder aggregates embedded in a continuous mineral matrix (Ratiarisoa et al., 2016). The impact of the binder type on permeability is less evident. Some results in the literature indicate that the nature of the binder matrix does not impact the vapour resistance of composites (Chamoin, 2013; Walker and Pavía, 2014); the large inter-particular spaces between hemp particles (macropores) have a greater contribution to permeability than the micropores (which are influenced by the hydraulicity of the binder) do. Grelat (2005), however, observed that the permeability of composites depends on the nature of binder. Testing four types of binder, he showed that the binder strongly influenced the permeability of hemp concrete.

Differences between experimental protocols for hygric characterization under dynamic conditions must affect the evaluation of the moisture buffering capacity. The higher temperature or air velocity can increase the water transfer in the porosity for highly permeable and capillary materials (Feng and Janssen, 2016; Ratiarisoa et al., 2016). Therefore, results available in the literature do not allow concluding on the overriding influence of a specific pore size range; the effects of binder matrix and aggregate natures cannot be properly assessed. Studying this aspect is one of the objectives of the present work. However, there is general agreement that the moisture buffer capacity of bio-aggregate-based building materials is high and classified as good or excellent according to the NORDTEST project (Collet and Pretot, 2012; Labat et al., 2016; Rahim et al., 2015, 2016; Ratiarisoa et al., 2016).

Furthermore, the thermal conductivity of bio-aggregate based building materials is strongly dependent on density. The increase in porosity decreases the density of the composite and consequently its thermal conductivity (Collet and Pretot, 2014). Thus, among other things, the characteristics of the binder and the particles used in the formulation significantly affect the thermal conductivity of vegetal concrete. (Amziane and Collet, 2017) and (Ratiarisoa et al., 2016) have summed up the considerable impact of the kind, origin, species, and processing of bio-aggregates on thermal conductivity. According to Walker and Pavía (2014), the binder type does not have a statistically significant impact on either thermal conductivity or specific heat capacity. On the contrary, Stefanidou et al., (2010) have highlighted the dependence of thermal conductivity on binder type. Their assessment suggests that lime binder is less conductive than cement and that the addition of pozzolanic materials reduces the thermal conductivity in comparison with pure lime.

As far as mechanical behaviour is concerned, the nature of both binder and bio-aggregates, as well as the bio-aggregate to binder ratio, strongly impact the composite strength (Chamoin, 2013; Ratiarisoa et al., 2016; Walker et al., 2014). In particular, chemical interactions can occur between lignocellulosic particles and a mineral binder, leading to poor mechanical performance. More generally, these interactions can disturb the setting and hardening of mineral binders, modify the properties of the composite and influence the durability of the material (Bourdot et al., 2018; Diquélou et al., 2015; Ratiarisoa et al., 2016).

The present article aims to evaluate the potential of maize and sunflower bark particles as a raw material in the design bio-aggregate based concrete. This study focuses on assessing the impact of both the aggregate-type and the binder-type on the hygric, thermal and mechanical properties of plant-based building materials. To do this, several characterization methods are used and compared. The first part of the article considers the properties of the raw materials: plant aggregates and binder pastes. The second part of the study is dedicated to the assessment of bio-aggregate-based concrete performance concerning porosity, compressive strength, thermal conductivity and hygric properties (sorption isotherms, water vapour permeability and moisture buffer value). The results are linked with those of raw material tests. This last part discusses the impact of the porosity of the constituents on the porosity of composites as well as the correlation between porosity and performance levels of composites during their use.

2 MATERIALS AND METHODS

2.1 Materials

2.1.1 Plant aggregates

For the last 15 years, hemp has been considered as the reference agricultural resource for an application in vegetal concrete. Although France ranked first among hemp producing countries in 2013, hemp has never been amongst the most widely available agricultural bio-products in the country (about 16 000 ha of hemp was cultivated in 2017 (InterChanvre, 2017)). Hence, it has become necessary to consider other possible sources of bio-aggregate available locally in greater quantities.

This study considers two different types agricultural by-products that are strong potential candidates to serve as aggregates in bio-aggregate based concrete: maize and sunflower bark chips. Unlike hemp, maize and sunflower are widely available in the south-west of France. The former is the second most cultivated cereal in France, with about 2.9 million hectares cultivated in 2016 to produce around 10 million tons of corn stalk per year; the latter is grown for its seeds, which provide vegetable oil, with about 614 000 ha cultivated nationwide, that is to say 230 000 tons of sunflower by-products available each year (GNIS; Laborel-Préneron et al., 2017).

The materials used here were obtained after harvesting, grinding and mechanical separation. In fields located in the Hautes-Pyrénées (France), stalks are harvested and leaves are pulled off manually. After a drying step, stalks are ground in a hammer mill equipped with a 32 mm diameter grid. In a final separation phase, a tilted conveyor belt and a blowing system are used to separate the pith from the bark, the two main layers of the stem from the centre to the outside of its cross section (*Figure 1*). Pith is collected for the production of insulated panels (Sidi Mohamed et al., 2017). The bark particles are then sieved using a 1 mm grid.

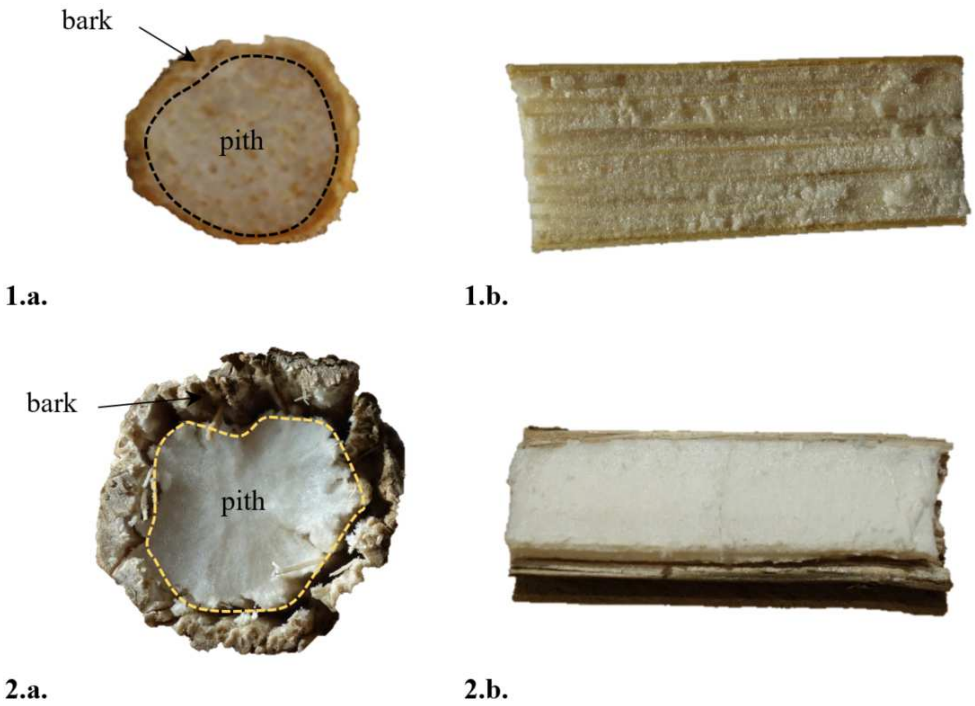

Figure 1 - Structure of maize (1) and sunflower (2) stem: photo of cross-section (a); longitudinal section (b).

2.1.2 Mineral binders

One of the main aims of this paper is to evaluate the impact of the nature of the binder on the hygric and mechanical performance of bio-aggregate-based concrete. Two different types of binder are considered: metakaolin-based pozzolanic binder and lime-based preformulated binder.

Metakaolin-based pozzolanic binder

The metakaolin used for this study was produced by flash calcination of kaolinite at 700 °C. Metakaolin is a pozzolanic admixture mainly composed of quartz, silicon and oxides of aluminium,

with an amorphous silico-aluminate mineralogical form. Like all pozzolanic materials, in the presence of water, metakaolin reacts with calcium hydroxide to form binding material. Thus, to formulate the binder, local metakaolin was combined with a commercial slaked lime in proportions determined to optimize binding properties (Dinh, 2014). Finally, to improve the performance of the composite at early age, potassium sulfate was added (2.9 % of the binder weight). K_2SO_4 is a chemical activator that encourages ettringite formation and accelerates the pozzolanic reaction (Dinh, 2014). Moreover, a super-plasticizer was introduced into water (1.65 % of the water weight) to improve mortar workability.

Lime-based preformulated binder

Air lime is obtained from pure limestone. Its calcination at about 900 °C produces quicklime according to a reaction that also produces carbon dioxide. Then, quicklime becomes slaked lime by hydration.

The hardening of lime-based mortar is based on the chemical reaction of carbonation. During this process, the carbon dioxide from the ambient air reacts with calcium hydroxide (lime) to form insoluble calcium carbonate:

$$Ca(OH)_2 + CO_2 \rightarrow CaCO_3 + H_2O$$

The hardening of air lime via this reaction is a mechanism with a net uptake of CO_2.

In this study, the lime-based preformulated binder used was a commercial binder designed for hemp concrete applications. According to the manufacturer's information, it contains 80 % of slaked lime and 20 % of hydraulic binder. Thus, this formulation combines hydraulic and air setting of lime-based mortar.

2.1.3 Design, manufacturing and properties of composites

This study investigates three bio-aggregate-based building materials having various formulations: two sunflower-concretes that differ by their binder and one maize-concrete made with the metakaolin-based pozzolanic binder.

Table 1 gives the mix proportions of the binder pastes while *Table 2* summarizes the mix proportioning of the concretes studied: Lime-Sunflower (LS), Metakaolin-Sunflower (MS) and Metakaolin-Maize (MM).

Table 1 - Mix proportioning of binder pastes for the production of one cubic metre of paste

Material	Binder (kg)	Water (kg)	W/B
Lime-based preformulated binder	1563	859	0.55
Metakaolin-based pozzolanic binder	1302	716	0.55

Table 2 - Mix design to produce one cubic metre of the bio-aggregate-based concretes studied

Material	Binder (kg)	Aggregate (kg)	Water (kg)	W/B	A/B
LS	374.3	161.9	390.4	1.11	0.43
MS	374.3	161.9	371.7	0.99	0.43
MM	374.3	161.9	288.8	0.83	0.43

Mix proportions of water were adjusted according to not only the water requirement of each binder to provide similar workability but also the aggregate water absorption capacity.

A procedure of blending adapted from the standardized one (EN 196-1) was applied to the binder pastes:

- 1 minute of mixing at 140 rpm;
- 30 seconds of mixing at 285 rpm;
- 30 seconds of cleaning out the bowl;
- 1 minute of rest;
- 1 minute of mixing at 285 rpm.

As far as bio-aggregate based concretes were concerned, the following method was employed:

- the bark was put in the mixer and water was then added for pre-wetting;

- the blend was mixed for 2 minutes;
- anhydrous components were then introduced and mixing water was added (with the superplasticiser if used). The blend was mixed until a homogeneous mixture was obtained;
- finally, the mould was filled by 3 layers, each compacted by vibration.

All concrete specimens were manufactured in cylindrical moulds 11 cm in diameter and 22 cm in length, while binder pastes were cast in 15 cm x 15 cm x 5 cm moulds.

Binder pastes were demoulded 48 hours after pouring. Binder paste materials, except for lime-based preformulated binder paste, were placed in sealed water-vapour-tight packs and stored at laboratory temperature: the cure hence took place under endogenous conditions. Specimens were cut 28 days later.

The moulds were removed from the concrete samples in two phases. First, the mould was opened at both ends of the specimen 7 days after concrete pouring. 48 days later, the samples were completely demoulded. The specimens were stored at laboratory ambient temperature and relative humidity conditions for 28 days. When cured, the specimens were cut into smaller samples according to the test requirements. The compressive performances of concrete were evaluated 60 days after demoulding, whereas their thermohygric properties were determined at least one year later.

2.2 Methods

2.2.1 Physical properties of plant aggregates

The following physical plant aggregate characterization tests are based on the protocol recommendations established by RILEM TC 236-BBM (Amziane et al., 2017).

Bulk density

The bulk density was found by weighing the aggregate and measuring the corresponding volume as described below. Three specimens of each plant aggregate were tested.

A cylindrical mould (here, 12 cm in diameter and 28.3 cm high) was half-filled with bark chips before being upended ten times. To obtain a horizontal surface, it was sometimes necessary to shake the mould slightly. A cardboard disc was then placed on the surface of the sample so that the level of material could be marked on the cylinder. The bark particles were then removed from the cylinder, which was filled with water to the level of the mark. Finally, the cylinder was weighed and the bulk density of aggregate (ρ in kg/m³) was calculated from the mass (m_{bark} in kg) and the volume (V in m³) of the sample according the following equation:

$$\rho = \frac{m_{bark}}{V}$$

with $V = \frac{m_{water}}{\rho_{water}}$

where ρ_{water} is the density of water (=1000 kg/m³).

Particle size distribution

The particle size distribution was studied in two-dimensions by means of image analysis using the freely available software ImageJ (National Institutes of Health, USA). This technique was particularly interesting as maize and sunflower bark chips are non-spherical particles. Thus, size distribution and morphology could be determined.

More than 2000 particles were analysed, covering an area greater than 100 pixels (i.e. greater than 0.18 mm² at 600 dpi resolution) for each bio-aggregate. Particles were scanned on a black background so that the contrast was maximised for image analysis. The images were subsequently binarized after which several geometrical parameters were determined: major and minor axis lengths, area, circularity, etc. The Equivalent Area Diameter (EAD), based on a particle of circular cross section, was calculated with the following equation:

$$EAD = \sqrt{\frac{4A}{\pi}}$$

with A, the cross sectional area of the particle (m²).

All the particle characteristics were then grouped into a single table to plot representative curves.

Water absorption of plant aggregates

Water absorption was measured by drying aggregates and then calculating their water content at a number of different immersion times. Three samples of about 30 g of bark chips were tested for each aggregate.

A synthetic permeable bag was immersed in water, to ensure complete wetting, before being placed in a salad spinner to remove water from the bag. The spinner was turned 100 times at approximately 2 rotations per second. The bag was then weighed.

After drying the specimens at 60 °C for a period of time long enough for the change in mass of the sample to be less than 0.1 % over 24 hours, the bark chips were cooled to ambient temperature in a desiccator. Then, they were placed in the spin-dried synthetic bag and immersed in water for a period of 1 min, 15 min, 4 hours, 24 hours or 48 hours. After each immersion time, specimens were placed in the salad spinner which was turned 100 times at approximately 2 rotations per second. They were then weighed.

For each time, the value of absorption (W in %) was calculated and the curve of water content versus logarithmic time was plotted:

$$W(t) = \frac{M(t) - M_0}{M_0}$$

with M(t) the mass (g) of the particles at a given time and M_0 the mass of spin dried bark chips (g).

2.2.2 Characterization of the porosity

The porosity of the materials was evaluated using three different methods: porosity accessible to water, mercury intrusion porosimetry and X-ray tomography. The first two techniques measure only the connected porosity of the sample.

Water immersion porosimetry

The Water Immersion Porosimetry (WIP) technique determines the total water-accessible porosity by saturating a sample with water and calculating the pore volume from the weight difference between the fully saturated and dry states (Arliguie and Hornain, 2007). To do this, samples are placed in a vacuum desiccator for 4 hours prior to being totally immersed (they must be at least 2 cm below the surface). The vacuum is maintained for 20 hours in the desiccator in order to fully saturate the samples with water.

The next step of the WIP measurement consists in weighing the saturated samples, first when they are submerged in water, then in air. A hydrostatic weighing system enables the immersed sample mass, M_{water} to be assessed. Then, samples are rapidly but carefully wiped with a wet cloth to remove surface water before the saturated weight in air (M_{air}) is measured. Both weight measurements are accurate to within $\pm$ 0.01 g.

Finally, samples are dried in an oven at 105$\pm$5 °C, until their weight has stabilized. The criterion for equilibrium is that the weight of a sample is sufficiently stable for two successive daily determinations (24 hours apart) of the weight of the test specimen to agree within 0.05 %. Once dried, samples are cooled in a desiccator to ambient temperature. The samples are weighed (M_{dry}) with an accuracy of 0.05 g.

Three specimens of each formulation were tested here. The apparent density, ρ_{ad} (kg/m^3), and porosity, φ (%), were determined from the same experimental sample and water density at room temperature θ (°C), $\rho_{water,\theta}$ (= 997.299 kg/m³ at 23.6 °C).

$$\rho_{ad} = \frac{M_{dry}}{M_{air} - M_{water}} \rho_{water,\theta}$$

$$\varphi = \frac{M_{air} - M_{dry}}{M_{air} - M_{water}} * 100$$

Mercury intrusion porosimetry

Mercury Intrusion Porosimetry (MIP) is a powerful method, which is used to explore the structure of pores larger than approximately 3 nm. It consists in applying pressure to force mercury into the

voids of a porous material, as mercury does not wet most substances and will not spontaneously penetrate pores by capillary action. The mercury fills the largest pores first. As pressure increases, the filling proceeds to smaller and smaller pores.

The Washburn Equation relates the applied pressure to the diameter of the pore (assumed to be cylindrical) using the contact angle between the mercury and the material, and the surface tension:

$$r = \frac{2\gamma cos\theta}{P}$$

r, radius of pores [m],
γ, surface tension of mercury [N/m],
θ, contact angle of mercury with the material [°],
P, imposed pressure [Pa].

Tests were performed using an AutoPore IV 9500 (Micromeritics) mercury porosimeter, which has a measuring range of 0.0007 - 420 MPa. Common values of γ and θ were used (Bourdot et al., 2017; Collet et al., 2008; Jiang et al., 2018): the mercury surface tension was 485 J/m² and the contact angle was 140°.The contact angle, θ, was assumed to be constant during intrusion and extrusion. Total porosity and pore size distribution were obtained over the entire operating diameter range (from 0.4 nm to 400 µm). Before testing, samples were dried in an oven at 50 °C.

Two samples of each material were tested to check that the mercury intrusion behaviour was similar for both.

X-ray tomography

X-ray tomography is a technique (Banhart, 2008) that enables inner inspection of a scanned object in a non-destructive way at sub-micron resolution. The sample is placed between an x-ray source and a detector. During an acquisition, a conical X-ray beam illuminates the sample and a series of 2D projection images is recorded for various sample orientations. The pixel values of each of the images correspond to the intensity of the transmitted X-ray beam and depend on the attenuation of the sample material. This relationship is expressed by the well-known Beer-Lambert law:

$$I = I_0 e^{-\mu h}$$

where I_0 is the incident X-ray intensity, I is the intensity remaining after the X-ray passes through a homogeneous sample of thickness h, and μ is the attenuation coefficient, which depends on the density and the atomic number of the sample material.

For non-homogeneous media, the product μh is replaced by a line integral along the X-ray path, yielding:

$$I = I_0 e^{-\int_0^h \mu(x)dx}$$

The recorded dataset of 2D projection images can be converted into a three-dimensional dataset, where every voxel (the three-dimensional counterpart of a pixel) corresponds to the linear attenuation coefficient of the physical material located at the voxel position. The analysis of the 3D distribution of the linear attenuation coefficients permits pores to be distinguished from the surrounding material matrix and their geometry and location inside the sample to be determined, together with derived quantities such as porosity, pore geometry and connectivity.

In this study, two tomographs are used to conduct the tomographic acquisitions, namely a Bruker SkyScan 1172 and a Zeiss Xradia Versa 510. The large detector size of the former enabled analysing relatively large samples of vegetal concrete at different resolutions, while the optical magnification system in the latter allowed for high-resolution scans of individual maize and sunflower bark chips. Three voxel sizes were selected (19.9, 10 and 4 µm) for the vegetal concrete acquisitions, permitting to obtain information at various scales (global concrete structures, arrangement of aggregate in concrete and interfaces between binder paste, aggregate and voids). The generator was respectively operated at 30 kVp with a voxel size of 0.74 µm for the bark chips; at 40 kVp with a voxel size of 4 and 10 µm and at 70 kVp with a voxel size of 19.9 µm for the MS concrete.

2.2.3 Hygric properties

Sorption isotherms

The relation between the water content of a material and the relative humidity of the environment at constant temperature can be represented by its sorption-desorption isotherm. Two specimens of each formulation were tested.

Dynamic Vapour Sorption (DVS) is a gravimetric technique that measures the amount of water that is adsorbed by a sample at equilibrium. First, the test specimens are dried in the DVS for 3 hours at 60 °C. The sorption isotherm is measured at 23 °C, according to the standard EN NF ISO 12571. The amount of water adsorbed is measured at successive stages of increasing relative humidity: 0, 20, 40, 60, 80 and 95 % RH. The water content is calculated from the mass of the specimen. For each step, moisture balance is considered to be reached in the specimen when the mass variation (in percentage) over the period of time (dm/dt) is less than 5.10^{-5} %/min over a ten-minute period or in a maximum time interval of 720 min for the first three steps, 1440 min for 60 and 80 % RH and 2160 min for the last step.

Water vapour permeability

Tests were performed on three cylindrical specimens of bio-aggregate-based materials 6 cm high and 11 cm in diameter. The wet cup method was applied as specified in standard NF EN ISO 12572. Before testing, samples were stored and initially in equilibrium with air at 23 ± 5 °C and 50 ± 5 % RH. The criterion for equilibrium was that the weight of the sample should have stabilized so that two successive daily determinations (24 hours apart) of the weight agreed to within 0.1 % of the mass of the test specimen.

The specimen was embedded at the top of the cup to avoid contact with the saline solution (*Figure 2*). Samples were then sealed to the support by a mix of 60 % beeswax and 40 % paraffin. Finally, the whole setup was surrounded by an aluminium tape at the junction of the support and the specimen. The whole system was placed in a climatic chamber regulated at 25 °C and 60 % RH and ventilated so that the air velocity at the surface of each specimen was greater than 2 m/s (in practice, from 2.3 to 3.2 m/s). The relative humidity in the cup was controlled by a saturated salt solution of potassium nitrate (93.6 % at 25 °C) while the relative humidity around the cup was controlled by air conditioning. The gradient of relative humidity created an outgoing flow of water vapour.

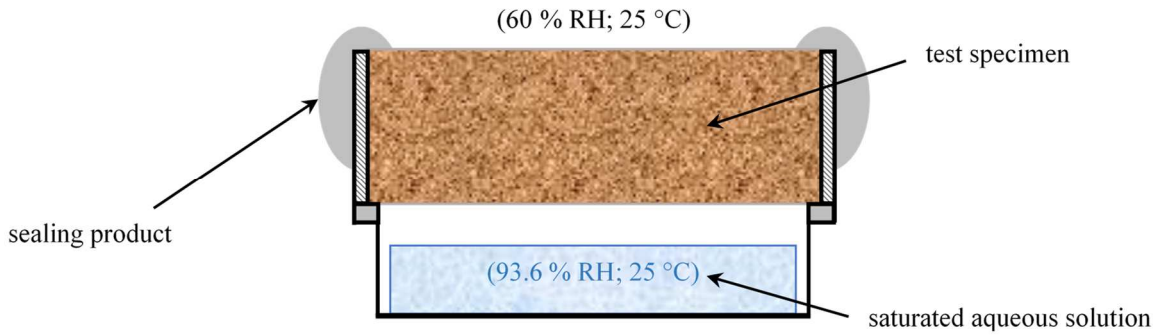

Figure 2 - Test cup scheme adapted from Vololonirina and Perrin (2016)).

The arrangements were weighed regularly until a steady-state vapour flux was reached. The transmission rate of water vapour through the sample, G, determined by linear regression of the kinetic of mass and the water vapour permeability, δ, was then deduced:

$$G = \frac{\Delta m}{\Delta t}$$

$$\delta = \frac{e}{\frac{A.\Delta p_V}{G} - \frac{d_a}{\delta_a}}$$

where G is the mass flow rate (kg/s); Δm, mass variation (kg); t, time (s); δ, water vapour permeability (kg/(m s Pa)); e, thickness of the specimen (m); A, exposed surface area (m²); Δpv, vapour pressure difference (Pa).

The vapour pressure was calculated with:

$$p_V = (RH_2 - RH_1) - 610.5 * e^{\frac{17.269\theta}{237.3+\theta}}$$

where RH_1 and RH_2 are the relative humidity inside and outside the cup, respectively (%); θ is the temperature (K) and δ_a is the water vapour permeability in air (kg/(m.s.Pa)). The air permeability can be expressed by the Schirmer formula. At 25 °C and standard atmospheric pressure, δ_a=1.96 10^{-10} kg/(m.s.Pa).

To be practically independent of temperature and pressure, a diffusion resistance factor μ was defined. The water vapour diffusion resistance factor corresponds to the ratio of the diffusion coefficients of water vapour in air and in the building material. Therefore, it represents the factor by which the vapour diffusion in the material is impeded, as compared to diffusion in stagnant air. For very permeable materials, such as mineral wool, the resistance factor is close to 1 whereas impermeable materials show a much higher value. For instance, polyethylene sheet resistance factor ranges from 50 000 to 320 000.

Moisture buffer value

The moisture buffering performance of a room is the ability of the materials in the room to moderate variations in the relative humidity. Thus, moisture buffering capacity is a hygric property by which hygroscopic materials in contact with the surrounding air adsorb and desorb moisture to create equilibrium with the relative humidity of the surrounding space. The NORDTEST protocol is one of the methods available for determining moisture buffering capacity.

Because of the change in relative humidity, the specimens will gain or lose weight. When the moisture exchange during one cycle is reported per open surface area and per % RH variation, the result is the practical MBV (kg/(m^2. % RH)):

$$MBV = \frac{\Delta m}{A.\left(HR_{high} - HR_{low}\right)}$$

Measurements were conducted on cylindrical specimens of bio-aggregate-based materials 6 cm high and 11 cm in diameter for each composition. The thickness of the samples was evaluated based on the notion of penetration depth. The penetration depth ($d_{p,1\,\%}$) is the depth where the amplitude of moisture content variations is only 1 % of the variation on the material surface. The moisture penetration depth is calculated using the following relation:

$$d_{p,1\,\%} = 4.61\sqrt{\frac{D_w t_p}{\pi}}$$

where D_w is the moisture diffusivity and t_p, the time period. The material thickness should be equal to or greater than the intended penetration depth.

Before testing, the test specimens were sealed on all but one side with aluminium tape. Then they were stored and initially in equilibrium with the air at 23 ± 5 °C and 50 ± 5 % RH. The criterion for equilibrium was that the weight of the sample should have stabilized to an extent that that two successive daily determinations (24 hours apart) of the weight agreed to within 0.1 % of the mass of the test specimen.

Two protocols based on the NORDTEST Project method were considered to evaluate the moisture buffer values of the three vegetal concretes. In both cases, the test specimens were placed in a climatic chamber, set to expose samples to a daily relative humidity cycle (8 hours at 75 % RH - 16 hours at 33 % RH), and their weight gains and losses were tracked with an accuracy of 0.001 g. An analytical balance with a resolution of 0.001 g, capable of weighing the test specimens was used. The temperature was kept constant at 23 °C. The first protocol consisted in monitoring the weight gains and losses of specimens continuously. To that end, the tested specimen was placed in the climatic

chamber, in an analytical balance permanently connected to a computer. The air velocity on the sample surface was about 0.2 ± 0.05 m/s, slightly higher than the velocity prescribed by the NORDTEST Project. The second method, consistent with the NORDTEST Project, involved manual weighing at various times of the cycle. The samples were placed in a climatic chamber so that the air velocity was about 0.1 ± 0.05 m/s and were removed from it to be weighed.

Figure 3 shows an example of the weight change response of one of the specimens measured when it was subjected to cycles causing the ambient humidity to vary between 33 % and 75 % RH for 16 and 8 hours, respectively.

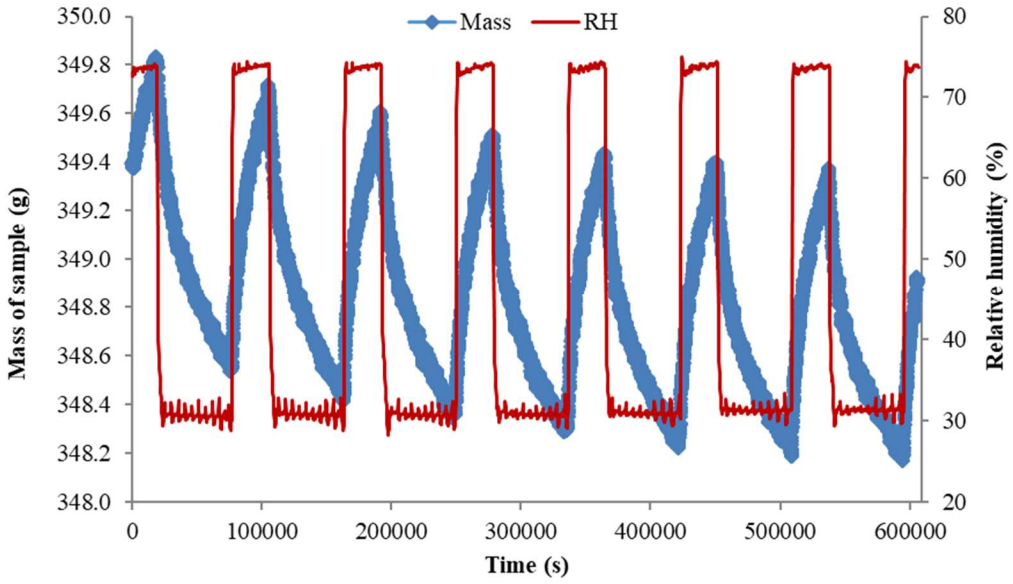

Figure 3 - Moisture uptake and release cycles for a sample. Exposure between 33 and 75 % RH.

The NORDTEST protocol determined the MBV value at steady state, i.e. when, for three consecutive cycles, the material satisfied the following conditions: change in mass, Δm (g) less than 5 % between the last three cycles; and difference between weight gain and weight loss within each cycle less than 5 % of Δm. In each cycle, Δm should be determined as the average between the weight gain during the moisture uptake branch of the cycle, and the weight loss during drying.

An ideal moisture buffer value (MBV_{ideal}), calculated under ideal surface transfer conditions, has been defined by Rode et al. (2005). It has a close relationship with the moisture effusivity (b_m), which is a parameter that can be derived purely from standard hygrothermal material properties. Thus, the theoretical or ideal MBV is given by the following equation:

$$MBV_{ideal} \approx \frac{G(t)}{\Delta HR} = 0.00568 * b_m * p_S \sqrt{t_P}$$

where $t_P^{½}$ is the square root of the time period ($s^{½}$)
p_S is the saturation vapour pressure (Pa)

$$b_m = \sqrt{\frac{\delta_P . \rho_0 . \frac{\partial u}{\partial \varphi}}{p_S}}$$

with δ_P, water vapour permeability ($kg.m^{-1}.s^{-1}.Pa^{-1}$)
ρ_0, dry density of the material (kg/m^3)
$\frac{\partial u}{\partial \varphi}$, hygric capacity (-).

Discrepancies existed between the measured material properties and the ideal value. The moisture effusivity is theoretically based on material properties which are determined under steady state and equilibrium conditions. However, the buffer property is a dynamic characteristic. The measurement method (under steady state or dynamic conditions) may influence the determination of MBV. Also,

differences between experimental and theoretical values may come from the transfer model, which might not fully describe the physical phenomena, or from the input data (water vapour permeability and sorption isotherm gradient), which might be flawed.

2.2.4 Thermal conductivity

The thermal conductivity λ was measured by a hot wire transient method. This technique consists in placing a shock probe between two pieces of material so that a power supply can be broadcast and the rise of temperature within the material may be measured.

Based on the heat conduction equation in cylindrical geometry, the thermal conductivity of the material can be obtained:

$$\Delta T = \frac{q}{4\pi.\lambda}(\ln(t) + K)$$

where Q is the heat flow per metre (W/m) and K is a constant including the thermal diffusivity of the material. Hence, there is a proportional relationship between temperature rise ΔT and logarithmic heating time ln(t).

This transient method only allows local measurements. To overcome the question of accuracy and representativeness for heterogeneous materials such as plant concrete, thermal conductivity is defined as the average of at least ten measurements. For each formulation, the device was placed at several locations on different samples. The spread of data resulting from all measurements was lower than 7 %.

The thermal conductivity was measured at room temperature (25 ± 2 °C) and a relative humidity of 50 ± 5 % RH. A Neotim-FP2C hot wire apparatus was used for this study. The heat flow and heating time were chosen so that a temperature rise higher than 5 °C and a correlation coefficient between experimental data and theoretical behaviour higher than 0.999 could be reached.

2.2.5 Compressive strength

The compressive strength tests on the specimens (11 x 22 cm²) were performed after 60 days of curing, using a 100 kN capacity hydraulic press. Four samples were tested for each formulation. The load was applied at a constant deflection rate of 3 mm/min while the unloading was carried out at 6 mm/min. The following 4-step loading cycle was applied to samples:

- loading up to 1 % of strain - unloading back to 0 %;
- loading up to 2 % - unloading to 0 %;
- loading to 3 % - unloading to 0 %;
- loading to 15 % for the sunflower-based material or 20 % for the maize-based one - unloading to 0 %.

The Young's modulus of each specimen was then calculated according to the "floating modulus" procedure from Niyigena et al. (2016), where the modulus is considered to be the mean of the maximum values obtained at the second, third and fourth loading steps.

3 RESULTS AND DISCUSSION

3.1 Raw material properties

3.1.1 Plant aggregates

Physical properties

The grading curves of maize and sunflower bark chips, according to the three main particle dimensions (minor and major axis, equivalent diameter (EAD)), are presented and compared in *Figure 4.a*. The circularity histograms for the particles, drawn on *Figure 4.b,* complete the shape analysis of the aggregates.

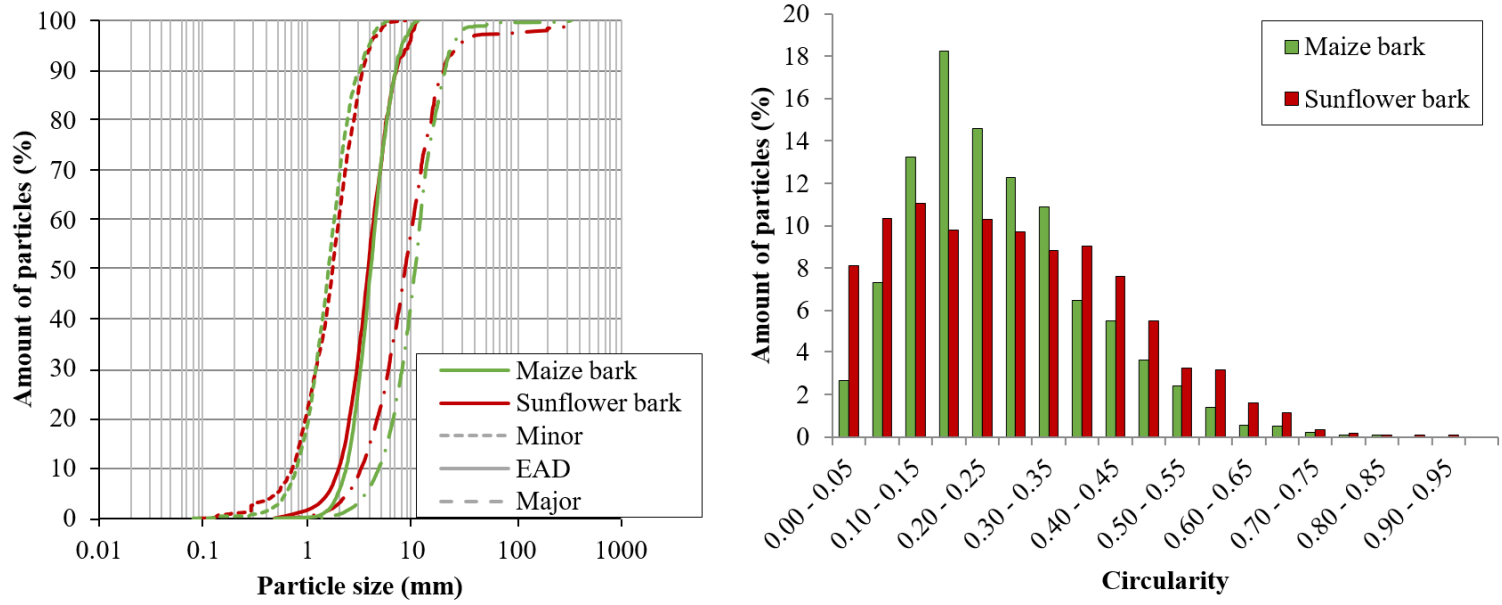

a. **b.**

Figure 4 - Particle size distribution (a) and circularity (b) of maize and sunflower bark chips.

The two aggregate grading curves show certain similarities: their particle size distributions are narrow and almost overlap. These observations are confirmed by the circularity distribution. The former reveals that maize and sunflower particles are elongated and have similar dimensions. The percentage of longer particles is slightly greater in the sunflower sample (*Figure 4.a.*) and the maize particles show a more elongated shape (*Figure 4.b.*). The shape characteristics could be adapted by changing the calibration process.

Bulk density measurements for plant aggregates were consistent with those in the literature (*Table 3*). The average value of the apparent density of the aggregates when loose and dry was 120.2 ± 1.0 kg/m³ 168.2 ± 4.5 kg/m³ for the sunflower particles and maize bark chips, respectively.

Table 3 - Apparent density of plant aggregates

	Corn cob	**Hemp shiv**	**Sunflower bark chips**	**Maize bark chips**
This study	-	-	120.2 ± 1.0	168.2 ± 4.5
Literature	450-500 (Eurocob, 2003; Laborel-Préneron et al., 2017; Verdier, 2012)	110-155 (Cérézo, 2005; Dinh, 2014; Laborel-Préneron et al., 2017; Nozahic, 2012)	95-170 (Brouard et al., 2018; Chabriac et al., 2016; Lenormand et al., 2014; Magniont, 2010; Nozahic, 2012)	-

The physical properties of the particles can explain the low density of the granular arrangements of maize and sunflower aggregates. The bulk density of bio-aggregates depends largely on the inter-particular porosity, which affects the compactness of the granular arrangement. It depends on the kind of material, its origin, its species and its processing (treatment, separation of woody core from fibre, particle size etc.). Thus, the greater percentage of long sunflower particles could lead to a looser granular arrangement than that found for maize bark particles.

Characterization of the porosity

Particles can be characterized by their highly porous structure, which is used to transport the sap of the plant. Two complementary methods were used to characterize the complex pore structure of bio-aggregates:

- X-ray tomography, to visualize pore shape and pore connectivity in three dimensions (*Figure 5*);
- mercury intrusion porosimetry, to quantify and view the pore size distribution (*Figure 6*).

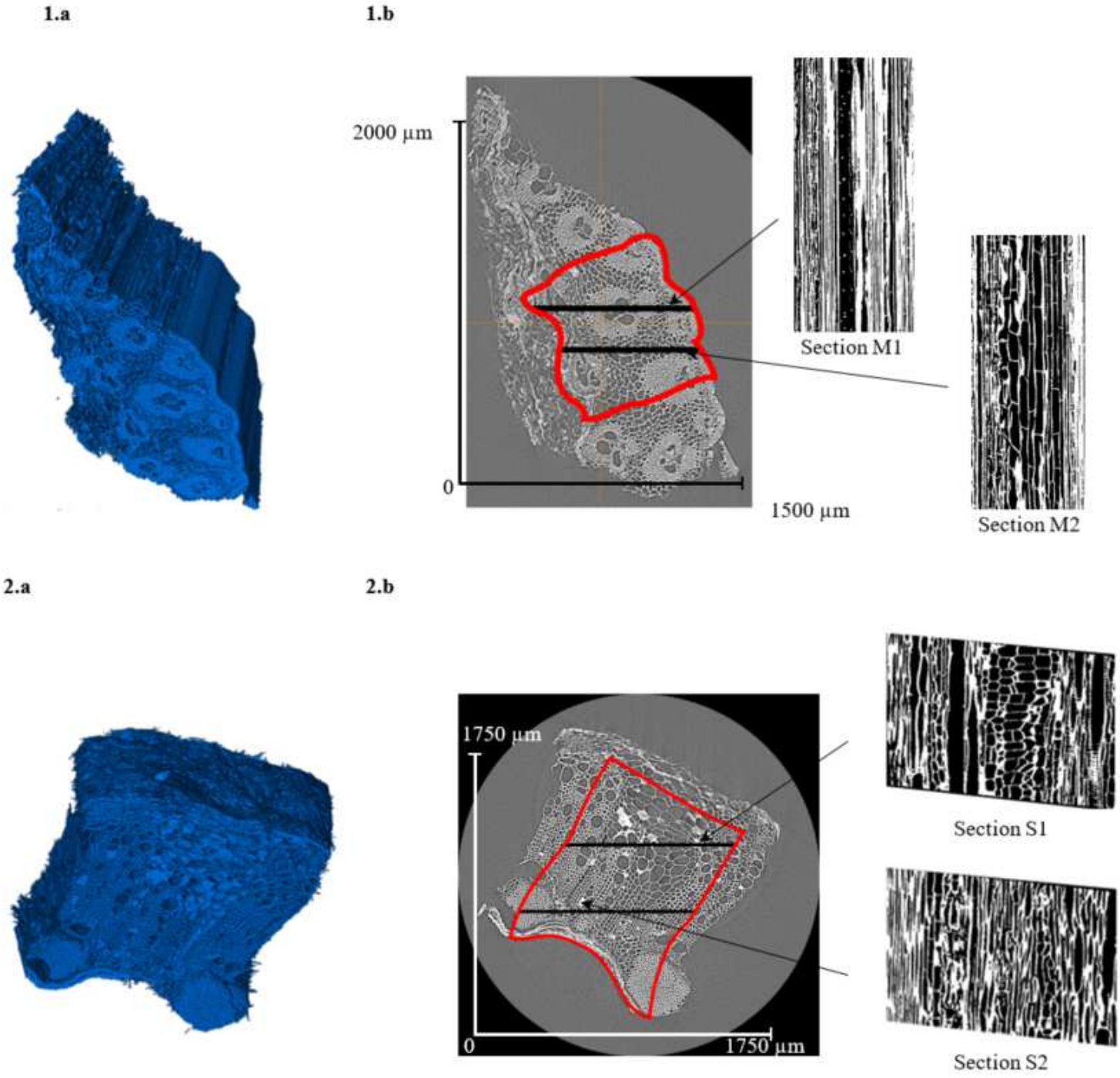

Figure 5 - 3D tomography reconstruction (a) and section images (b) of maize (1) and sunflower (2) samples. The red contour delimits a representative unit cell of the material.

An analysis of representative 3D unit cells of maize and sunflower bark chips revealed both a tubular and an alveolar structure. Both porosities were strongly connected. The pore structures exhibited a main family of fine sized pores and large diameter vessels interconnected throughout the structure.

Table 4 summarizes the average accessible porosity estimated by image analysis and the MIP method.

Table 4 - Total aggregate porosities determined by X-ray tomography and MIP

	Maize bark chips	Sunflower bark chips
Average accessible porosity estimated by X-ray tomography (%)	51 ± 9	58 ± 8
Average accessible porosity measured by MIP (%)	64.3 ± 0.8	75.2 ± 1.7

MIP and X-ray tomography provide coherent and complementary data: mercury intrusion porosimetry gives an indication that pores exist with sizes well below the resolution of the X-ray scan; X-ray tomography, detecting both open and closed-porosity, is a more reliable source of information for pores with equivalent diameter greater than 3 µm.

Studying the pore size distribution obtained (*Figure 6*) epitomizes the overlapping area of the two used techniques: both methods detect a peak in the 10-80 µm range sizes. Moreover, the techniques agree on the fact that maize particles are less porous than sunflower bark chips. The results reported here are lower than values from the literature. Mostly obtained by Mercury Intrusion Porosimetry (MIP), gas pycnometry or calculation, the estimated porosity from previous studies for diverse vegetal bark and pith particles ranges from 75 to 99 % (Bouasker et al., 2014; Bourdot et al., 2017; Chabriac et al., 2016; Jiang et al., 2017, 2018; Nozahic, 2012; Rahim et al., 2015, 2016).

However, neither of those methods provide a perfect description of the porosity network. Those bias are responsible for the gap between the values obtained by X-ray tomography and MIP. This difference is consistent with characterization results for bio-based carbon foam in Merle et al. (2016). Several causes can explain this outcome. Firstly, degradation of the particles due to the pressure applied by MIP, greater than the compressive modulus of the agricultural by-products, is possible. Porosity measurements based on MIP will then be overestimated. Secondly, the scan resolution of the X-ray tomography technique tends to underestimate the total porosity: pores smaller than the resolution (here around 3 µm) cannot be distinguished. Thirdly, the selected unit cell also impacts the obtained porosity: given the wide range of cell sizes the porosity will be underestimated if a too low proportion of small pores is present in the unit cell.

Figure 6 presents the relative area distribution of pores obtained from X-ray tomography and the differential intrusion distributions from mercury intrusion porosimetry, for both maize and sunflower particles. As the samples per material show a very comparable pore size distribution for MIP method, even though there are variations in peak heights, only one pore size distribution is presented.

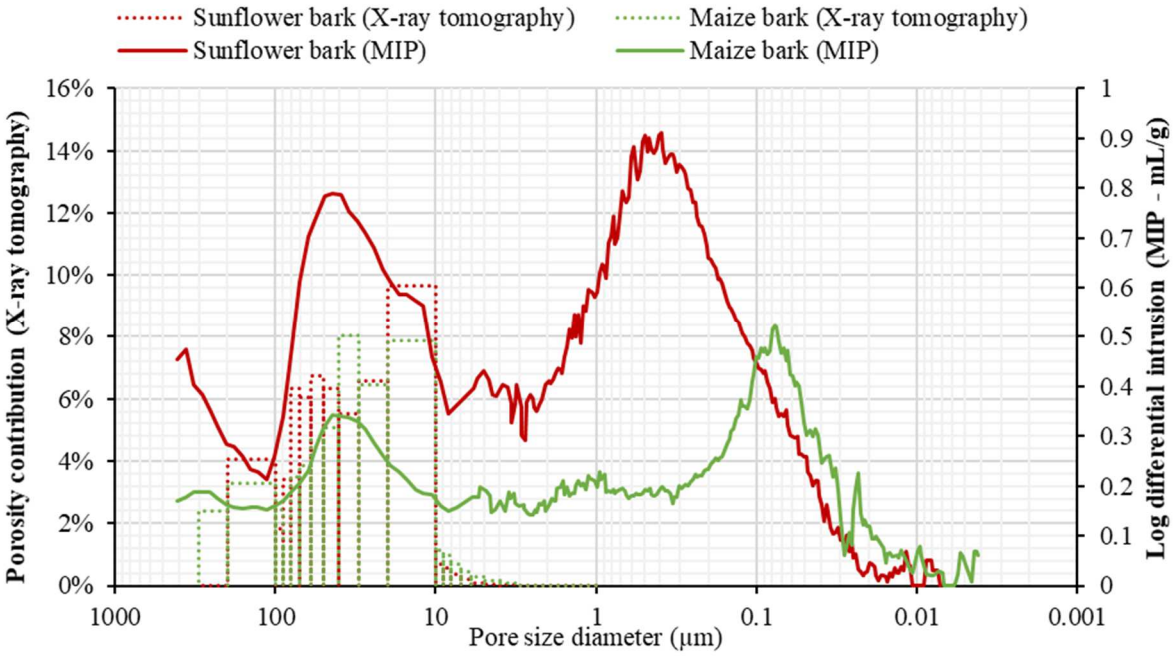

Figure 6 - Pore size distribution of plant aggregate samples determined by X-ray tomography and mercury intrusion porosimetry.

The two plant aggregates present a wide range of pore sizes. Their differential intrusion graphs show a bimodal pore size distribution with two clearly separated peaks. The main pore radius for sunflower ranges from 0.1 µm to 1 µm while the range is about 0.07-0.1 µm for maize. The second peak is common to the two types of bark chips and is between 10 µm and 70 µm. The results above show similarity with the bimodal distribution of hemp shiv (Jiang et al., 2017, 2018). These authors reported that, for hemp particles, a principal peak is located between 0.03 to 1 µm probably due to the pit membrane voids, pit apertures and other small voids between cell walls. A second peak is present in the 20-80 µm range, corresponding to the macro-voids produced by the vessels.

The MIP measurement gives information that is complementary to the X-ray tomography study since it can detect smaller pores. Thus, the pore size distribution determined by MIP reveals a second range of pores, non-identifiable by image analyses. This distinction between the two techniques explains the underestimation of the total porosity by X-ray tomography. However, as underlined in Merle et al. (2016) quantitative pore size analysis obtained by MIP has to be qualified, as accessible voids are detected with sizes ranging only from 0.4 nm to 400 µm. Moreover, the pore structure may be destroyed during the test. Finally, the ink-bottle effect yields an erroneous distribution: the volume of large pores accessible only via a narrow opening is recorded as a large number of small pores having the size of the opening. The ink bottle effect thus causes a systematic bias towards small pores.

Moisture storage capacities

In order to evaluate the impact of the highly porous structure of maize and sunflower bark chips on their hygric behaviour, two tests were performed: water absorption and vapour sorption capacity measurements. The former is an important formulation parameter as competition may occur between the particle absorption and the matrix hydration. Hence, it can lead to greater water requirement. *Figure 7* presents the absorption kinetics of the two particle types evaluated for up to 48 hours.

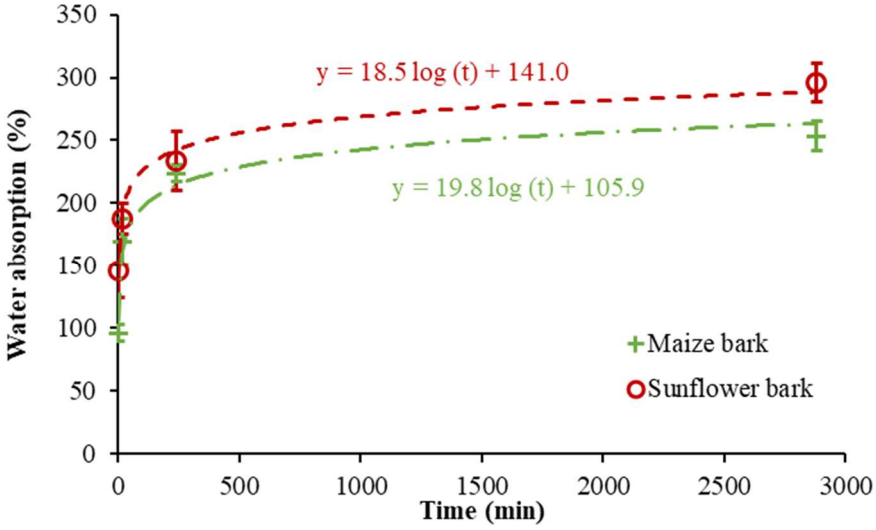

Figure 7 - Absorption capacity of the studied plant aggregates with time.

The two plant aggregates present high water absorption capacities after 48 hours of immersion: the maize bark chips and sunflower particles have gained up to 254 % and 296 %, respectively, of mass of water. They demonstrate fast kinetics of absorption since, after only 4 hours of immersion, maize and sunflower particles reach respectively 79 and 88 % of their 48-hour retention abilities. The retention capacity of sunflower bark chips is similar to that of hemp shiv (Dinh, 2014; Flament, 2013; Nozahic, 2012) and significantly lower than that of lavender straw (Ratiarisoa et al., 2016).

The kinetics of water absorption for plant particles is modelled in Nozahic (2012), where a simple time-dependent relation is established to characterize the phenomenon of absorption in the bio-aggregate particles:

$$W(t) = C_A.\log(t) + W_0$$

where W_0 is the initial water absorption on the surface of the particle (kg/kg) and C_A is the coefficient of water absorption by the particle (kg/log(s)).

This modelling points out the similar absorption rate, about 19 kg/log(s), of the two plant aggregates and highlights the distinct initial water absorption of the bio-aggregates. After 1 minute of immersion, sunflower particles have retained 146 % of water by mass while maize has only absorbed about 96 %. Hence, maize concrete requires a lower quantity of water than sunflower composite, an observation that pleads in favour of the use of maize particles as aggregates in vegetal concrete.

Thanks to a dynamic method, the sorption isotherm up to 95 % RH was determined for both bark chips (*Figure 8*).

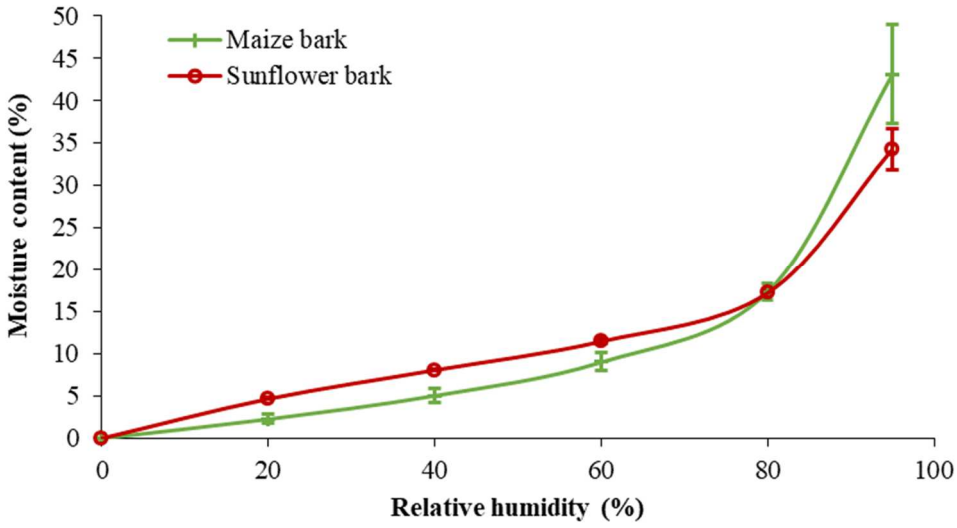

Figure 8 - Sorption isotherms of maize and sunflower bark particles.

Like most ligno-cellulosic materials, maize and sunflower particles have high water contents (Bouasker et al., 2014; Laborel-Préneron et al., 2017; Magniont, 2010). The sorption curves of the two aggregates are type II and III sigmoidal isotherms, respectively, according to the IUPAC (International Union of Pure and Applied Chemistry) classification (Sing, 1985). Those two types of isotherms are commonly obtained for bio-aggregates (Bouasker et al., 2014; Laborel-Préneron et al., 2017).

For low to medium relative humidity, the water content shows slightly higher values for sunflower bark chips than for maize aggregate. At 40 % RH, water content is about 8 % for sunflower bark particles while it is only 5 % for maize bark chips. In the capillary condensation domain, the rate of increase in water content is greater for maize particles than for sunflower aggregate, leading to significantly higher water content at 95 % RH. The maximum water contents for the two types of bark chips are high: the sorption value of maize particle is about 43 %, which is higher than that of sunflower bark chip (34 %) in the capillary condensation range (above 80 % RH).

The highly porous structure of maize and sunflower bark chips contributes to their water sensitivity. The greater open porosity of sunflower results in higher mixing water requirements than those of maize aggregates as well as higher water vapour adsorption capacity up to 80 % RH. In the capillary condensation domain, the greater number of smaller pores in maize particles, than in sunflower bark chips, is responsible for the steeper slope of the water uptake curve. The sorption isotherm results obtained are typical for mesoporous and macroporous materials (i.e. with pores that are 2 nm in diameter or larger), which is consistent with the observations.

The addition of such aggregates to a mineral matrix could lead to an increase of the sorption capacity of the composite material.

3.1.2 Binder pastes

Physical properties

Tests performed on binder pastes showed that metakaolin and lime-based binders had similar bulk density values, respectively 1079 ± 1 kg/m³ and 1052 ± 106 kg/m³. The values were determined by means of hydrostatic weighing. A problem with the immersion of one lime-based specimen was responsible for the higher standard deviation compared with metakaolin-based binder.

Characterization of the porosity

To better understand the values of bulk density of matrix pastes, the porosity of each material was evaluated. *Table 5* presents and compares the open porosity of the two binders studied, using two methods described in section 2.2.2: WIP and MIP.

Table 5 - Open porosity of binder pastes estimated by WIP and MIP.

Material	Water accessible porosity (%)	Mercury accessible porosity (%)
Metakaolin-based binder	56.2 ± 0.1	54.4 ± 0.8
Lime-based binder	54.8 ± 4.6	53.4 ± 1.8

It is clear that, regardless of the method by which they are determined, lime and metakaolin-based binder pastes have porosities that are of the same order of magnitude, i.e. about 55 %. These findings are in line with the bulk density values presented above and in the literature. Previous experiments have found that lime paste porosities range from 50 to 64 % (according to the water to binder ratio) (Cérézo, 2005). Nozahic (2012) estimated the accessible porosity of a pozzolanic binder paste at 54 %.

The results obtained from the two techniques are quite similar for both binders, porosities obtained by absorption of water being 3 % higher than those obtained by MIP. Similar differences were found by other authors for cement and lime-based binder pastes (Arandigoyen et al., 2005; Goyer, 2007; Krus, 1997; Tracz, 2016). On the one hand, this may be due to the fact that binder paste contains pores smaller than 0.4 nm and larger than 0.4 mm, which cannot be identified by MIP. On the other hand, WIP does not reflect the real open porosity of the material because water, a strongly polar liquid, is adsorbed by the binder gel as so-called interlayer water. Its molecules slip in between the mineral layers of the calcium silicate hydrate (C-S-H) phases, thus increasing the distances between them and forming additional porosity (Tracz, 2016). This phenomenon involving C-S-H, present to a limited extent in metakaolin and lime-based matrices, explains the slight discrepancy between the two total porosity estimations.

On the same grounds as above, only one pore size distribution per binder paste is presented in *Figure 9*.

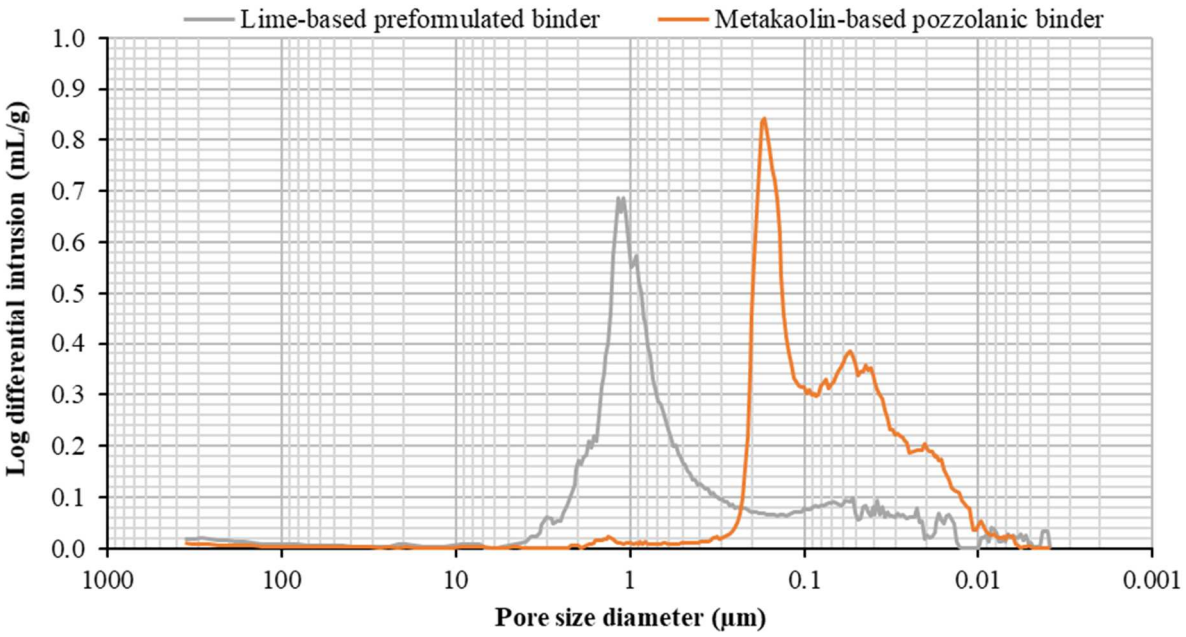

Figure 9 - Pore size distribution of binder paste samples determined by mercury intrusion porosimetry.

The pore size distribution curves show that the pastes are very different in morphology but they both have a predominant unimodal distribution. Lime-based preformulated binder paste shows a narrow range of pores: all pores are smaller than 3 µm and most of them have a diameter around 1 µm. The results achieved are in agreement with previous works on lime-based pastes (Arandigoyen and

Alvarez, 2006; Arandigoyen et al., 2005; Nunes et al., 2016). Regarding pozzolanic paste, the pore size distribution indicates that a majority of pores have diameters between 0.1 and 0.2 µm. A complementary porosity in the range of 0.01-0.1 µm, close to the one detected by Nunes et al. (2016), is clearly visible.

Hygric properties

Figure 10 gives the sorption isotherms of the two binder pastes.

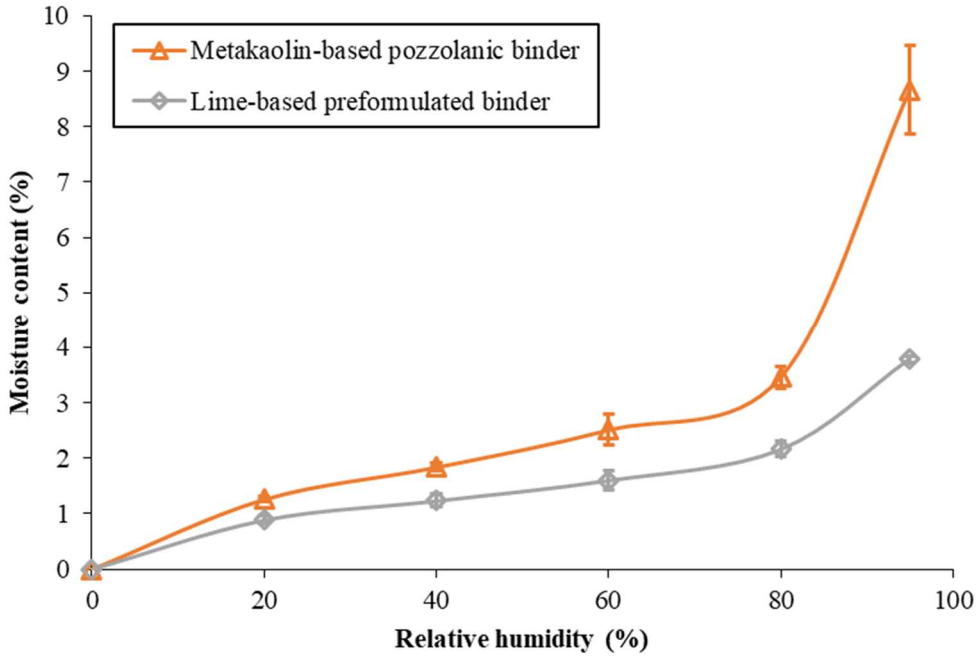

Figure 10 - DVS water vapour sorption isotherm of the two binder pastes at 23 °C.

The shape of the sorption curves corresponds to a sigmoidal isotherm, type II according to the IUPAC classification.

The pozzolanic matrix shows a higher water sorption capacity than lime-based binder paste over the entire range of relative humidity. This gap widens as the hygrometry increases, due to the fact that capillary condensation occurs sooner in the finer pores of the pozzolanic binder than in the lime-based binder porosity. The reduced pore size in metakaolin paste may induce a larger specific surface than that of the lime-based paste and increase its capacity for mono and polymolecular adsorption.

For relative humidity higher than 60 %, as the specific surface area of pastes increases remarkably with pozzolanic addition to lime paste (Černý et al., 2006; Nunes et al., 2016), the water uptake is much greater for metakaolin-based binder than for lime-based matrix. At 95 % RH, while the water content of metakaolin-based binder is 8.7 %, for lime-based binder paste it is only 3.8 %. The addition of pozzolan to lime paste significantly affects the pore size distribution: the main peak is shifted from the 0.1 - 1 µm region to 0.01 - 0.1 µm. This results in a greater water vapour sorption capacity of pozzolanic-based binder than of lime paste, especially in the capillary condensation domain. This occurs because pores within lime-based binder paste are not fully saturated at the highest relative humidities. A large part of this paste's porosity consists of large pores with diameters around 1 µm, in which it can be assumed that capillary condensation does not occur in equilibrium with 95 % RH.

As the total porosities of both binder pastes are very close, continuing the relative humidity increment until equilibrium at 100 % is reached can be expected to lead to similar moisture contents at the matrix saturation point. This behaviour was recorded by Garnier (2000): at low and medium humidity ranges, the water vapour sorption capacity of lime-based pastes is low, while a strong, abrupt growth is observed for the highest relative humidity (Samri, 2008).

3.2 Composite performances

3.2.1 Porosity

The open porosity of bio-aggregate based building materials was measured by MIP tests. Results are presented in *Table 6*.

Table 6 - Open porosity of composites estimated by MIP method

Material	Open porosity (%)
Lime-Sunflower	68.6 ± 1.7
Metakaolin-Sunflower	71.5 ± 5.3
Metakaolin-Maize	69.2 ± 0.7

The total porosity of maize and sunflower concretes are about 70 %. The formulation does not have a statistically significant impact on the measured porosity. The high porosity of vegetal concrete is consistent with values found in the literature. Several authors have explored the porous structure of bio-composite, mostly for hemp concrete, and have found porosity ranging from 60 to 80 % (Cérézo, 2005; Chamoin, 2013; Collet et al., 2008, 2013; Driss; Evrard, 2008; Glé et al., 2011; Gourlay et al., 2017; Rahim et al., 2016), depending on the formulation and the method of determination.

Figure 11 shows the pore diameter distribution of maize and sunflower concretes. As mentioned previously, only one result is presented per material.

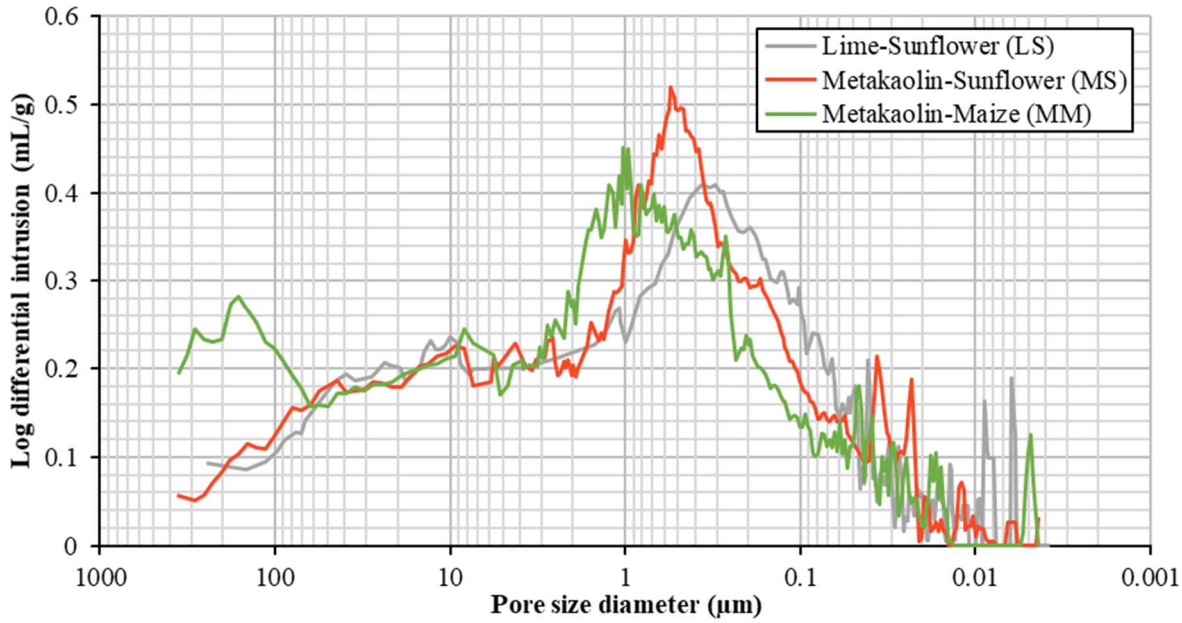

Figure 11 - Pore size diameter distributions of the maize and sunflower concretes.

Figure 11 shows that, in the range explored by mercury porosimetry, the vegetal concretes have a multi-scaled porosity, which matches the conclusions of previous studies (Cérézo, 2005; Chamoin, 2013; Collet et al., 2008, 2013; Dubois, 2014; Evrard, 2008; Glé et al., 2011; Lawrence et al., 2012). All distributions show a predominant peak between 0.1 and 1.1 µm. For the MM composite, the pore size distribution also presents a family of large pores, with a diameter greater than 60 µm. The latter pore range does not appear for the sunflower-based concretes.

Figure 11 also compares the influence of raw materials, both binder and bio-aggregate types, on the pore size distribution of bio-aggregate based building materials. Pore size distributions of sunflower concretes show that LS and MS curves overlap over a wide range of pore diameters. In particular, it highlights the pore size range of sunflower particles at about 0.5 µm. Some differences can be noticed in the additional porosity range (0.1 - 1 µm), where MS shows a higher peak than LS, and in the range of 0.01-0.1 µm, corresponding to the metakaolin-based matrix complementary porosity. The impact of the nature of bio-aggregates on the pozzolanic-based composite plotted on the same figure shows that the two curves are close but with some variations. On the one hand, the graph

confirms that MM concrete has a greater number of pores larger than 100 µm than MS composite does. This could be due to the more elongated shape of maize particles leading to a different granular arrangement of particles. On the other hand, MS material shows a greater volume of micropores. This is consistent with the higher proportion of pores between 0.1 and 1 µm in sunflower bark chips.

The porosity within the binder paste is more difficult to detect on the pore size distributions of concretes. This might be due to the fact that the volume of binder paste capillary pores increases because of an excessive dose of water or it might be due to a sampling problem leading to binder paste around the vegetal particles being under represented. Additional porosity to that provided by raw materials in the micron-range appears in all composite distributions: there are capillary pores attributable to the vaporization of excess water, air entrapment during mixing or the arrangement of particles.

3.2.2 Hygric behaviour

Sorption isotherms

Vegetal concretes are highly hygroscopic materials. *Figure 12* gives the adsorption isotherms of the three maize and sunflower concretes studied.

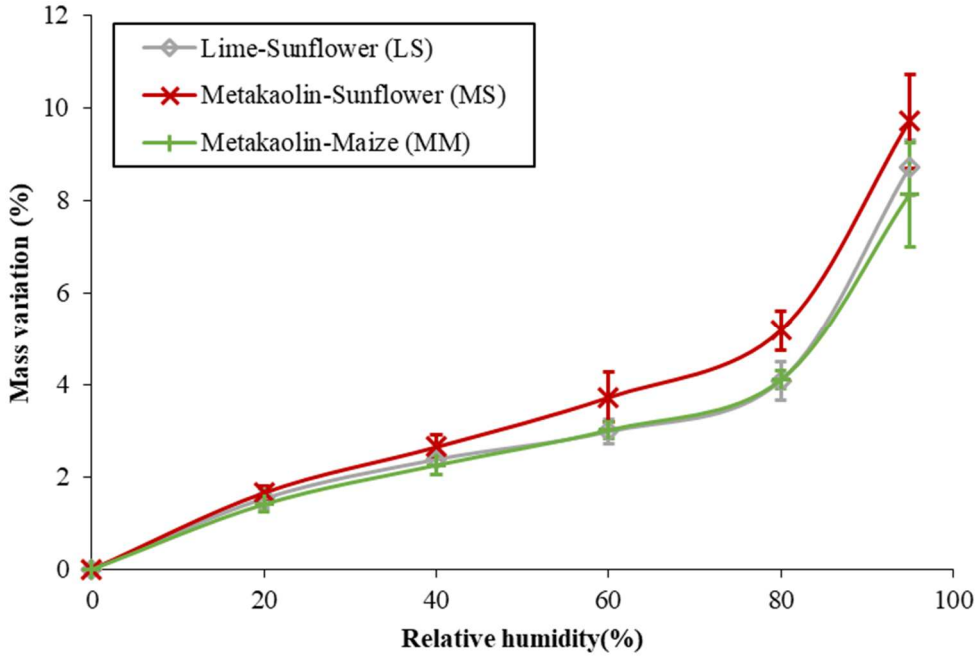

Figure 12 - Sorption isotherms of composites.

This figure shows that the adsorption isotherms of the three materials display a similar pattern. The curves correspond to type II isotherms according to the IUPAC classification, which is in agreement with macroporous materials. Their water contents at 20, 40, 60 and 80 % RH are similar to those of vegetal concretes encountered in the literature (*Figure 13*). In the capillary condensation domain, however, the water uptakes of LS, MS and MM composites are lower than the outcomes predicted by previous studies. This reflects a failure to achieve the equilibrium state at the highest relative humidities. Similar values to that reported in the literature should have been obtained if the test had been pursued until the saturation point was reached.

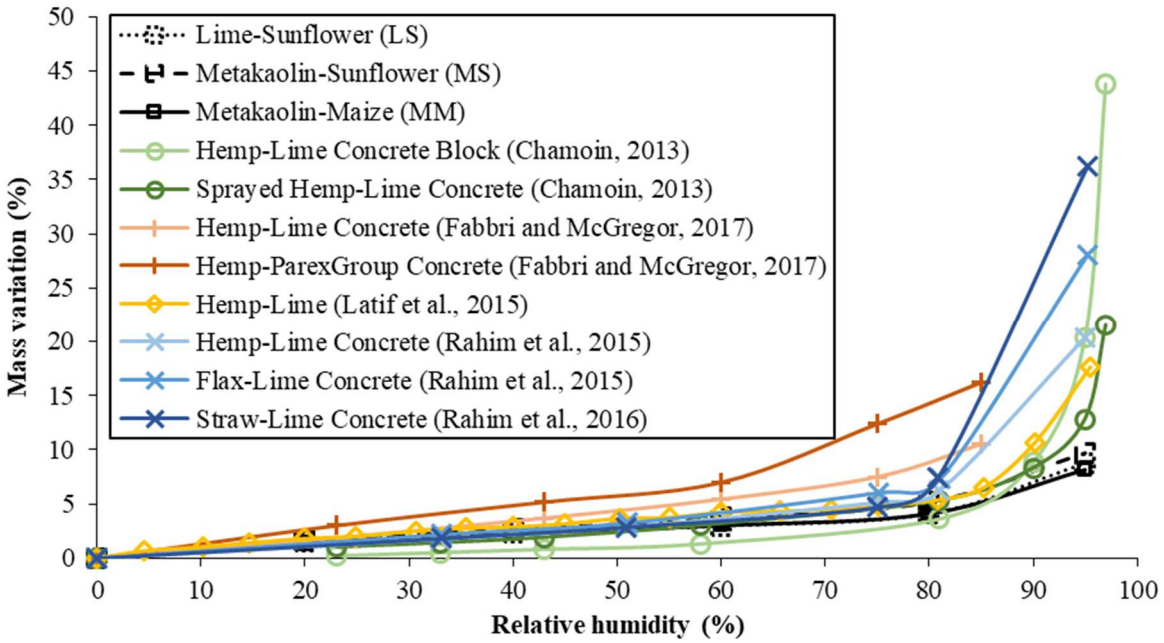

Figure 13 - Results from literature of mass variation of vegetal concretes with the relative humidities.

The water content of the composites studied is of the same order of magnitude as that of the binder pastes, between two and five times smaller than bio-aggregates' water sorption capacity. Thus, studies on the sorption capacity of concretes reveal a significant impact of the binder nature on the moisture sorption potential of bio-based materials. However, the effect of plant particle types is also noticeable. In the literature, research works have recorded stronger effects of both bio-aggregates and binder types on outcomes, particularly in the capillary condensation domain (Chamoin, 2013; Collet et al., 2013; Rahim et al., 2015, 2016; Walker and Pavía, 2014). These two parameters largely affect the sorption isotherm curves of vegetal concretes. In the present study, analysis of bio-aggregate based concretes brought out the impact of binder and aggregate types on their sorption isotherms over the entire range of relative humidity.

When the two binder matrices are compared, the results are consistent with the water sorption of binder pastes alone (see section 3.1.2): lime-based materials show a lower water adsorption capacity than metakaolin-based materials. As far as metakaolin-based materials are concerned, the nature of the bio-aggregates is observed to have a noteworthy impact: MS concrete shows a higher sorption isotherm slope than MM material from 20 to 80 % RH. This result is in accordance with the relative sorption capacity of the two bio-aggregates between 20 % and 80 % RH (see section 3.1.1). Nevertheless, at 95 % RH, the maize-based composite sorption capacity remains below that of sunflower-based composite, unlike the sorption capacity of their respective bio-aggregates. A hypothetical explanation could be that the larger pores of maize bark particles, in which capillary condensation occurs for high levels of humidity, could be filled with the binder paste in the composite. The limited effect of formulation on sorption curves is consistent with the close values of open porosity in the three composites studied.

Water vapour permeability

The average water vapour permeability and water vapour diffusion resistance factor of maize and sunflower concretes are set out in *Table 7*.

Table 7 - Average water vapour permeability and resistance factor of maize and sunflower concretes

	Water vapour permeability, δ_p (kg/(m.s.Pa))	Water vapour diffusion resistance factor, μ (-)
LS	$7.67 \times 10^{-11} \pm 1.66 \times 10^{-11}$	2.62 ± 0.57
MS	$1.46 \times 10^{-10} \pm 1.68 \times 10^{-11}$	1.35 ± 0.16
MM	$1.42 \times 10^{-10} \pm 2.20 \times 10^{-11}$	1.40 ± 0.20

Diffusion resistance values are much lower than observed by Collet et al. (2013), Evrard (2008), Rahim et al. (2015, 2016); and Walker and Pavía (2014), which range from 5 to 12 for hemp, rape straw and flax concretes.

This difference with the literature is probably attributable to experimental conditions, which could have a very large impact on the values obtained. With the cup method, Vololonirina and Perrin (2016) studied the influence of different test parameters such as thickness and area of the specimen, thickness of the air gap at the lower surface of the specimen, air velocity, cup height, and hygrometry inside and outside the cup. Especially for hygroscopic materials such as bio-aggregate based building materials, the water vapour permeability is strongly linked to the local relative humidity. Thus, measurements of water vapour permeability, which are performed at different levels of relative humidity (dry-cup and wet-cup), may result in different values for one and the same material. The increase of the water vapour permeability with relative humidity was proved by Chamoin (2013) and Collet et al. (2013): the water vapour permeability diffusion coefficient increased by a factor of seven depending on the hygrometry. This may have been due to surface diffusion and capillary condensation, which become noticeable at higher humidities.

It seems that the nature of the binder matrix significantly affects this hygric property, while the effect of aggregates is not measurable. In the present study, lime-based concrete's permeability (7.67×10^{-11} kg/(m.s.Pa)) was found to be about half that of metakaolin composites (1.42×10^{-10} - 1.46×10^{-10} kg/(m.s.Pa)). It appears that the greater volume of pores in the micron-range (0.5-1 µm) directly impacts the permeability. In the literature, Chamoin (2013) and Walker and Pavía (2014) do not report a statistically significant effect of the type of binder on the water vapour permeability of hemp concrete, whereas Tran Le (2010), referring to Grelat (2005), observed that a less hydraulic binder led to a higher water vapour diffusion resistance factor. From a bio-aggregate point of view, the results in this research reveal that the moisture diffusion coefficient of metakaolin-based concretes is close to 1.5×10^{-10} kg/(m.s.Pa) regardless of the particle type. Thus, the nature of the aggregate does not have a discernible effect on water vapour permeability. This finding is in line with work (Chamoin, 2013) pointing out that different treatments of hemp shives (fibred or defibred) lead to similar values of permeability in hemp concrete.

Moisture buffer value

Figure 14 gives the moisture buffer values of vegetal concretes calculated from the last three cycles.

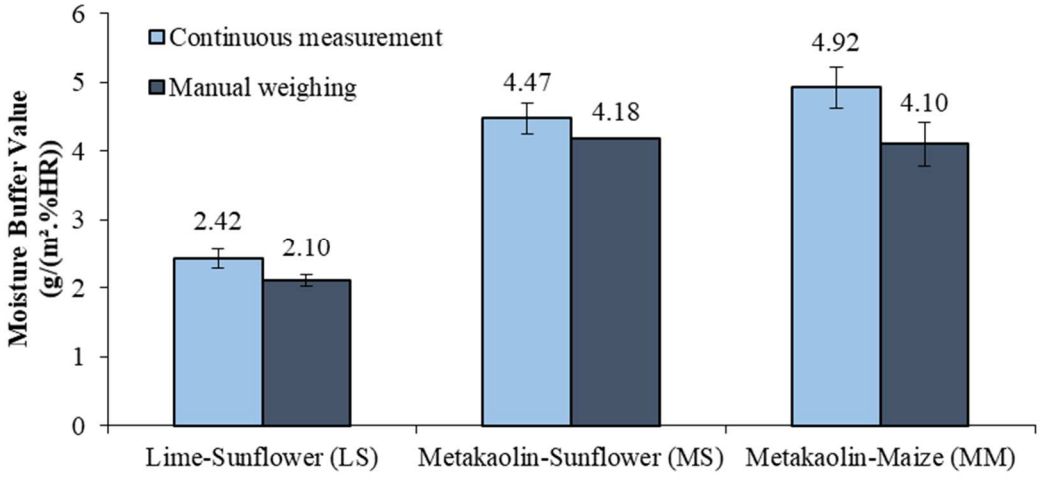

Figure 14 - Moisture buffer values of vegetal concretes.

The values are in the range 2.10-4.92 g/(m². % RH), lime concrete (2.10-2.42 g/m². % RH) showing lower values than metakaolin-based concretes (4.10-4.92 g/(m². % RH)). According to the NORDTEST Project classification, the moisture buffering capacity of the three bio-aggregate based materials is excellent. Consequently, they can be considered as excellent hygric regulators that improve hygrothermal comfort.

Lime-Sunflower composite shows an MBV similar to those measured experimentally (Collet et al., 2013; Tran Le, 2010) and analytical estimations made by Evrard (2006) and Tran Le (2010). Very few references in the literature report an MBV exceeding 3 g/m². % RH for vegetal concrete. Ratiarisoa et al. (2016) have studied metakaolin-based hemp and lavender concretes. The resulting values (3.5-3.85 g/m². % RH for composite including lavender aggregates and 3.12 g/m². % RH for hemp concrete) largely exceed other values found in studies for hemp concrete.

According to Tran Le (2010), MBV_{ideal} is statistically 1.42 times higher than the MBV measured for an applied exposure changing sinusoidally. This seems to be verified in our case (*Table 8*).

Table 8 - Practical and ideal moisture buffer values

	Practical Moisture Buffer Value (g/m². % RH)	**Ideal Moisture Buffer Value (g/m². % RH)**	**MBV_{ideal}/1.42 (g/m². % RH)**
LS	2.10-2.42	3.6	2.6
MS	4.18-4.47	5.7	4.0
MM	4.10-4.92	5.1	3.6

The hygric regulator capacities of concretes are consistent with the results obtained previously. The moisture buffer value is proportional to the moisture effusivity of the material, which is linked to the moisture permeability and to the derivative of the sorption isotherm (Rode et al., 2005). Lime-Sunflower has the lowest derivative sorption curve and is the least permeable material. Thus, its moisture buffer value (2.10-2.42 g/m². % RH) is logically lower than that of metakaolin vegetal concretes (4.10-4.92 g/(m². % RH)). This gap can be interpreted as the impact of binder type on MBV: metakaolin composites seem to be better hygric regulators than lime concretes. This confirms results found by Ratiarisoa et al. (2016) on metakaolin-based concrete, which largely exceed values found for hemp-lime concrete. The assessment does not allow any conclusion to be drawn on a significant impact of plant particle porosity and shape on the moisture buffering capacity of bio-based materials. However, it should not be forgotten that methods in previous studies did not always respect the recommendations of the NORDTEST procedure; the impact of environmental conditions can be partly responsible for variations of MBV.

The comparison between the two MBV measurement protocols underlines the influence of the environment. The manual weighing protocol leads systematically to 6 to 17 % lower MBV than the continuous method. The air velocity on the surface of the specimens, the disturbances caused by frequent opening of the climatic chamber and the change of environment during weighing (when outside the climatic chamber) may well contribute to the variations in the hygric regulator capacity of materials and hence affect the results.

3.2.3 Thermal conductivity

The thermal conductivity values of the three composites are shown in *Table 9*.

Table 9 - Thermal conductivity of the vegetal concretes

	Density (kg/m³)	**Thermal conductivity (W/(m.K))**
LS	539.64 ± 51.56	0.127 ± 0.008
MS	511.07 ± 61.86	0.128 ± 0.009
MM	534.08 ± 82.30	0.112 ± 0.006

Thermal conductivity values of maize and sunflower-based concretes are about 0.11-0.13 W/(m.K). These composites can therefore be considered as self-insulating materials. In the literature, hemp

concretes in the same density range are found to have similar thermal conductivity values, from 0.115 for lime-hemp concrete (de Bruijn and Johansson, 2013; Evrard, 2008), to 0.122 for metakaolin-based concrete (Dinh et al., 2012).

Thermal properties are dependent on density (*Figure 15*). Cérézo (2005) established a relationship between increasing thermal conductivity λ and rising density ρ of hemp concrete. This equation can be generalized to vegetal concretes:

$$\lambda = 0.0002\rho + 0.0194$$

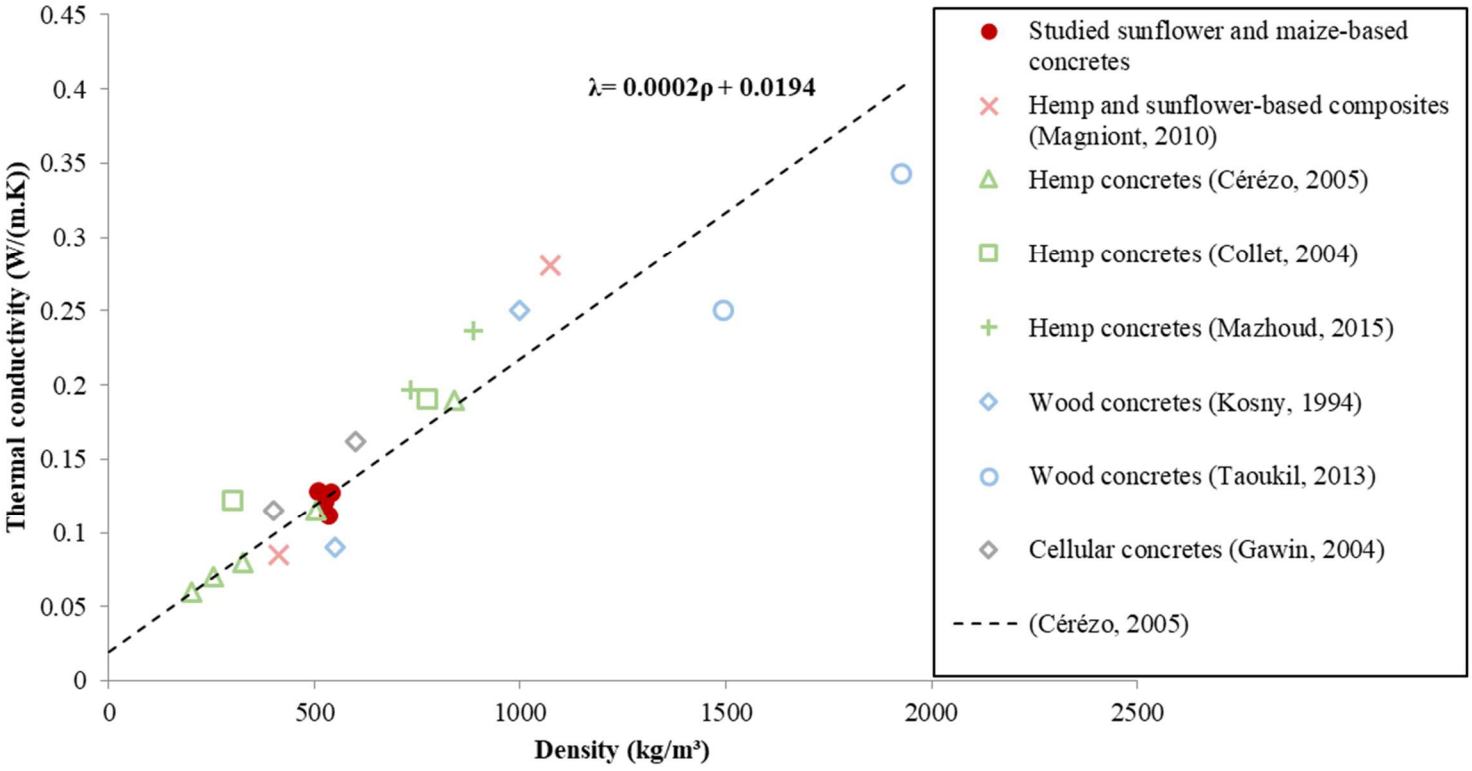

Figure 15 - Relationship between density and thermal conductivity of building materials and relationship established by Cérézo (2005).

The results show that thermal conductivity increases linearly with density. The concretes appear to have a thermal conductivity similar to that predicted from the relationship above.

The outcomes for thermal conductivity seem to underscore the critical impact of the macro-porosity of vegetal concretes rather than the meso- and micro-pores of both bio-aggregates and binder pastes. The sunflower concretes are not statistically affected by the binder type, even though the insulating properties of the binder pastes are plainly distinct (*Table 10*). This conclusion on the role of the matrix in the thermal conductivity of composites is in accordance with those of Walker and Pavía (2014) but differ from those of Gourlay et al. (2017), the latter finding that thermal conductivity varies significantly with the type of binder.

Table 10 - Thermal conductivity of the two binder pastes studied

	Density (kg/m³)	**Thermal conductivity (W/(m.K))**
Lime-based preformulated binder	1 052 ± 106	0.366 ± 0.008
Metakaolin-based pozzolanic binder	1 079 ± 1	0.277 ± 0.002

On the other hand, the metakaolin-based composites show a slight dependency on the bio-aggregate type, with a trend toward greater insulating properties of MM compared to MS: maize-based concrete values being 12.5 % lower than those of sunflower composite. Thus, the granular arrangement of particles as well as the vaporization of excess water are responsible for the creation of millimetre width pores. Such pores increase the insulating capacity of materials. Hence, the binder

type does not affect the thermal properties whereas the larger inter-particular porosity of MM (underlined by MIP tests) leads to lower thermal conductivity values than MS.

3.2.4 Compressive strength

Vegetal concretes are not able to bear major strains but they are capable of deforming significantly. The compression loading curves are shown in *Figure 16* for the concretes investigated.

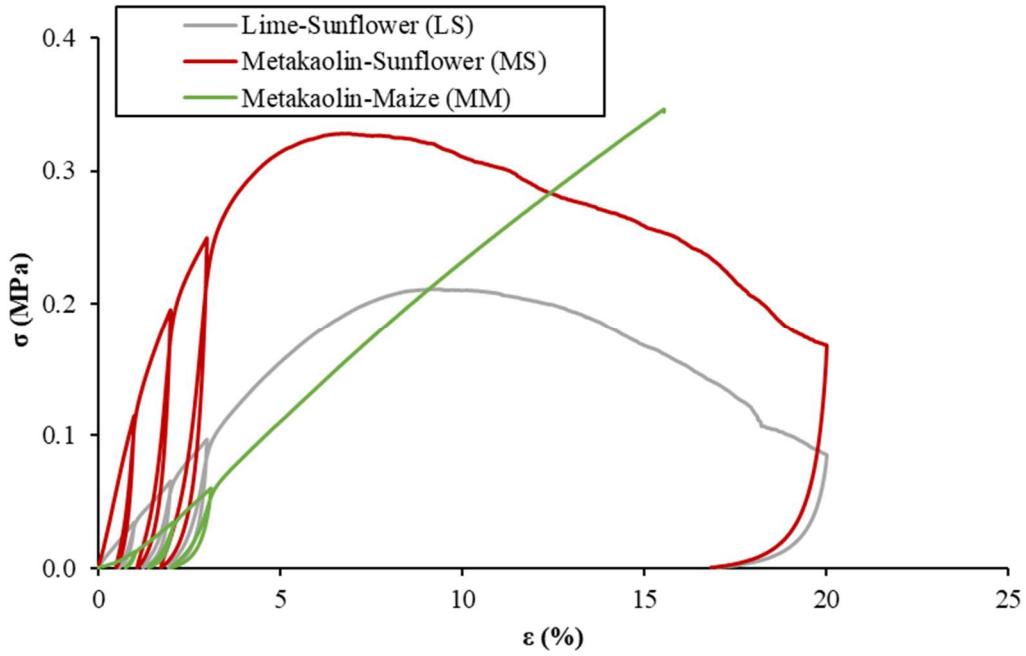

Figure 16 - Compressive strength tests on vegetal concrete formulated with different types of binder or bio-aggregate.

The types of binder and of plant aggregate play a role in modifying microstructural properties of materials. Their mechanical performance, highly dependent on their microstructure, can also be modified.

When the impact of the type of binder is compared for sunflower-based composites, the LS concrete shows a poorer mechanical performance than the MS one. This is consistent with results of the stress-strain behaviour of metakaolin-based pozzolanic binder and lime-based preformulated binder pastes alone. These findings can explain the increase of strength of lime-based mortars containing pozzolans, since the shrinkage reduction should result in the elimination of cracking around aggregates in mortars (Nežerka et al., 2014).

Despite their different compressive strength, the sunflower-based concretes show graphs that are similar to those of the behaviour of hemp concrete found in Arnaud and Gourlay (2012) and Cérézo (2005), where the stress-strain curve can be divided into three regions:

- a first part of the curve where the material presents a linear quasi-elastic behaviour. During this phase, the binder matrix, which is stiffer than vegetal particles, supports the compressive stresses and slight strains are recorded;
- in a second part, the curve increase is smaller, which indicates that the behaviour of vegetal concrete becomes elastoplastic. Zones of stress concentration appear between the particles, the binder matrix cracks gradually and the particles are crushed little by little. The curve finally reaches a maximum: the compressive strength σ_{max} of the specimen;
- finally, the binder matrix is completely damaged and no longer plays a mechanical role. The bio-aggregates now support the most compressive stresses. The strain levels are high and the stress levels decrease because the particles are less stiff than the binder.

The two concretes formulated with metakaolin-based binder reached a maximum stress of about 0.33 MPa but showed radically different mechanical behaviours. Unlike sunflower formulations, the maize concrete compresses continuously on load application. Thus, the material is highly deformed by the strain. Under pressure, the particles rearrange, whereas the binder matrix does not play any

mechanical role. The strain-stress curve is similar to that of vegetal aggregates alone, characterized by high deformation (Amziane and Arnaud, 2013; Arnaud and Gourlay, 2012; Niyigena et al., 2018). The variability of maize composites' performances is probably due to the poor adhesion between the bio-aggregates and the binder matrix. Maize water-soluble components have a strongly deleterious effect on the setting and the hardening mechanisms of the pozzolanic binder, as evidenced by (Bourdot et al., 2018). It prevents the concrete from setting and modifies the mechanical behaviour of hardened concrete.

From a quantitative point of view, the identification of compressive strength is not uniquely defined for bio-based materials. Thus, arbitrary decisions are made by the authors, leading to a great variability of approaches for measuring it (*Table 11*). In that respect, Mazhoud et al. (2017) understand the compressive strength as the transition between reversible behaviour and compacting behaviour. So, the compressive strength is established as the stress corresponding to a change of slope on the strain-stress curves. In our study, this parameter is not applied as it is impossible to detect a slope change for the MM material: the concrete deforms irreversibly from the beginning of loading (Arnaud and Gourlay, 2012; Cérézo, 2005; Niyigena et al., 2016). Nguyen (2010) considered stresses measured at two strain levels: 1.5 % and 7.5 %. When a maximum stress is reached before the strain reference values, it is this maximum strength that is recorded. Some authors have also established the compressive strength as the maximum stress of the material and the strain at failure corresponding to this maximum of stress. As it is meaningless to keep the maximum value measured for maize-based composite, the 15 % deformation stress is also considered.

Table 11 - Compressive strength identification methods applied to the materials studied

	LS	**MS**	**MM**
σ_{max} (kPa)	201.8 ± 32.7	326.2 ± 18.5	-
$\sigma_{\varepsilon=1.5\ \%}$ (kPa)	45.2 ± 6.4	132.8 ± 23.7	26.9 ± 10.0
$\sigma_{\varepsilon=7.5\ \%}$ (kPa)	182.2 ± 17.4	324.4 ± 20.2	174.9 ± 15.2
$\sigma_{\varepsilon=15\ \%}$ (kPa)	173.4 ± 44.1	228.4 ± 58.9	329.6 ± 21.2

Previous studies on manually vibro-compacted hemp concretes have obtained globally similar values of compressive strength. Arnaud and Gourlay (2012) showed values of compressive strength between 0.35 and 0.85 MPa for hydraulic lime and pre-formulated lime-based binder; Cérézo (2005) found hemp concrete strength ranging from 0.25 MPa to 1.15 MPa. The maximum compressive strength was evaluated to lie between 0.32 MPa and 0.45 MPa by Niyigena et al. (2016). Depending on the binder employed, the maximum stress of hemp concrete varied between 0.1 MPa and 1 MPa for Murphy et al. (2010) and ranged from 0.29 and 0.39 MPa at 1 year for Walker et al., (2014).

Likewise, the calculation methods found in the literature to determine the Young's modulus are also different. The study by Niyigena et al. (2016) defined the most suitable method as the calculation of the elastic modulus based on the mean value of the strongest increase in the strength/strain ratio recorded at each loading stage. The floating modulus method applied to maize and sunflower concretes leads to the values presented below (*Table 12*):

Table 12 - Floating modulus of LS, MS and MM concretes

Materials	LS	MS	MM
E (MPa)	26.6 ± 1.2	55.1 ± 6.7	14.7 ± 2.7

Results from Niyigena et al. (2016) show mean values of Young's modulus for hemp concrete ranging from 28.81 MPa to 44.01 MPa. Findings from the present study are thus within the range of elastic modulus given in the literature. Values vary depending on the type of binder, the nature of the aggregates and the compaction level.

To better understand the stress-strain behaviour of materials, X-ray tomography measurements were conducted. First, the poor interface between the plant particles and the binder paste was studied (*Figure 17*).

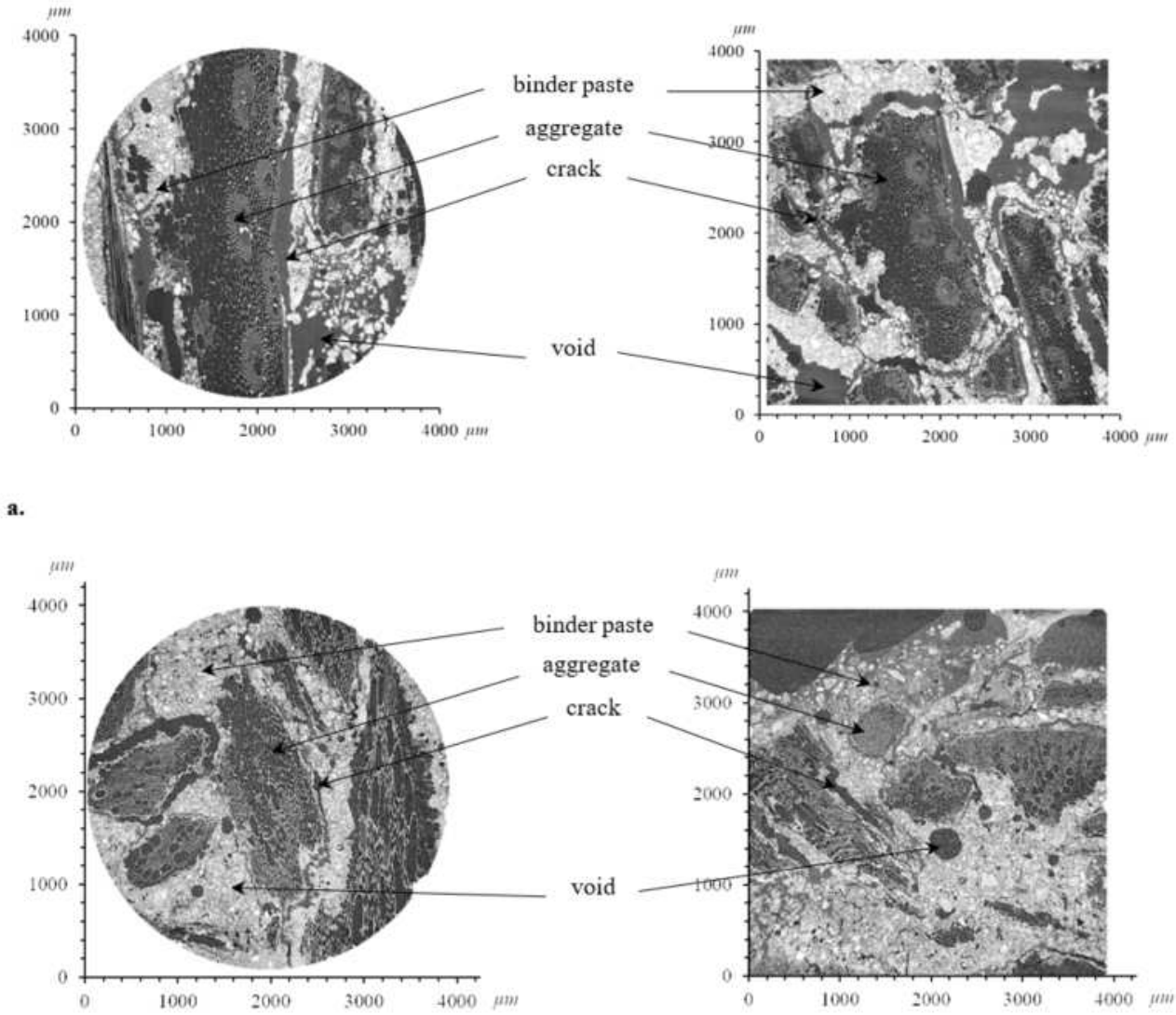

Figure 17 - X-ray tomography images of (a) maize and (b) sunflower metakaolin-based concretes (voxel size of 4 µm).

The tomographic observation of metakaolin-based concretes revealed the presence of shrinkage-induced cracks at the interface between the bio-aggregates and the binder paste. Shrinkage occurs when the concrete is exposed to a drying environment, which causes an increase in tensile stress leading to cracking in the absence of external loading (Day et al., 2013). The shrinkage of concrete is influenced, in particular, by the amount of water present in the fresh concrete: the higher the amount of mixing water is, the greater are the drying shrinkage and number and size of the resulting cracks.

Next, the anisotropic internal arrangement of vegetal concretes is known to give rise to anisotropic physical properties. Some works have underlined the impact of bio-aggregate orientation on thermal and mechanical properties (Elfordy et al., 2008; Hustache and Arnaud, 2008; Nguyen et al., 2010). Thus, it appeared interesting to analyse the spatial orientation of the particles within the metakaolin-based concretes. Because of contrast issues, only the MS composite allowed the bark chips to be extracted, enabling the shape and spatial orientation of bio-aggregates within the binder matrix to be determined, as shown in *Figure 18.a*.

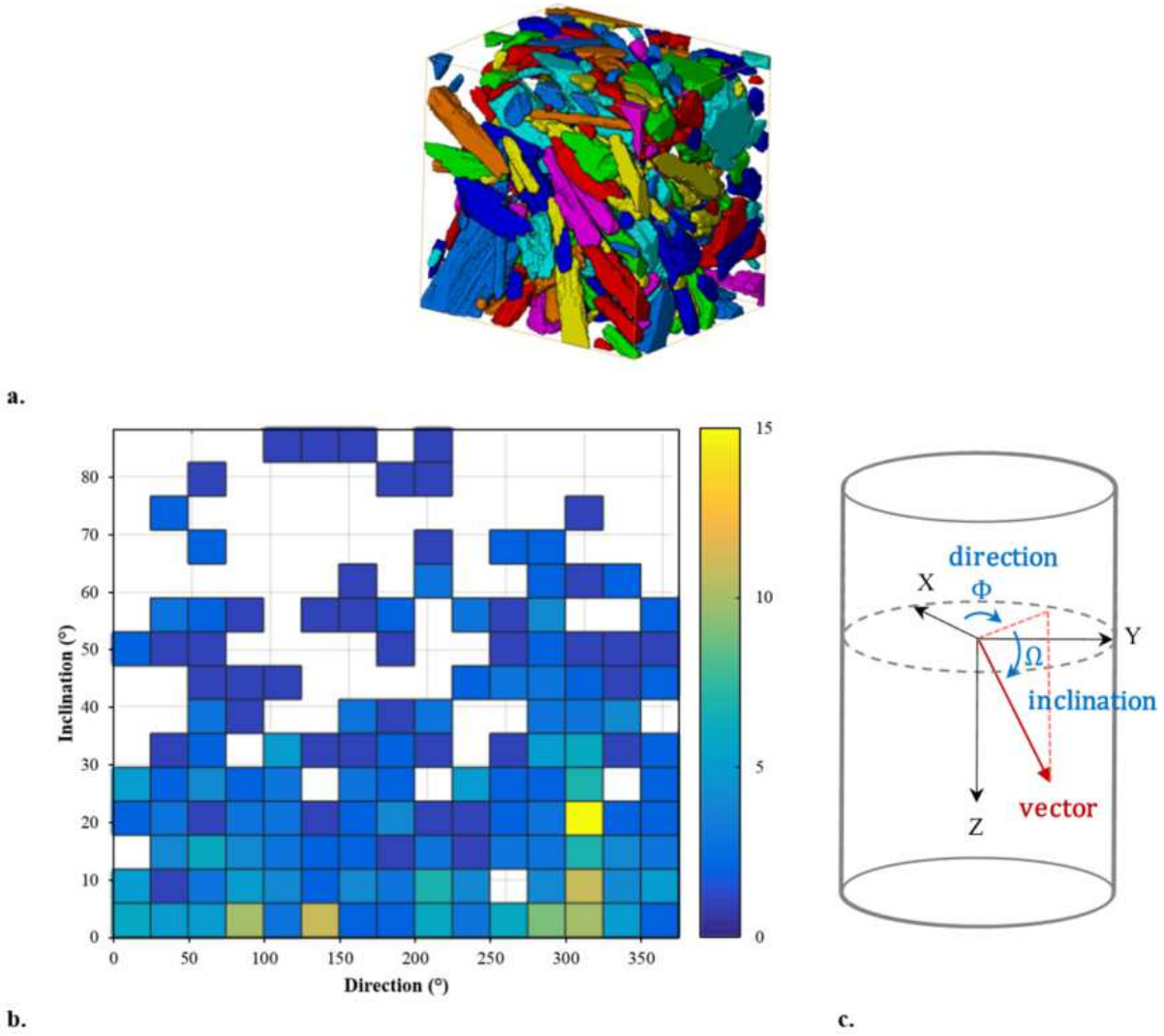

Figure 18 - (a) 3D reconstruction of the sunflower aggregates within the metakaolin binder paste (voxel size of 19.9 µm) and spatial orientation of particles: (b) 2D normalized histogram of direction versus inclination and (c) definition of direction and inclination.

Figure 18 shows the particle inclination with respect to a horizontal plane versus its projected in-plane orientation. The applied convention is depicted schematically in *Figure 18.c.* It can be observed that the great majority of aggregates exhibit no preferential in-plane direction but do show an inclination of less than 40° from the horizontal. This can be attributed to the compaction applied during the casting process directing the elongated particles towards stratified planes transverse to the compaction direction, also corresponding to the compressive strength direction This observation is in line with previous works (Williams et al., 2016, 2018).

4 CONCLUSION

The results presented here point out the lack of standard procedures or common approaches, which lead to arbitrary decisions and thus to a large diversity of results in the literature. The impact of testing conditions on the performances of bio-based materials in use is also underlined in this study.

Exploration of the shape and inner porosity of plant aggregate particles by X-ray tomography appears to be a promising technique as it enables inner inspection of the microstructure in three dimensions in a non-destructive fashion. X-ray tomography is a powerful tool, which can easily be combined with other techniques and help to characterize the microstructure of vegetal concretes.

The overall porosity of bio-aggregate particles, combined with the meso and micro-porosity of binder paste, directly affects the pore size distribution of the composite. All this adds up to a new

category of pores attributable to the vaporization of excess water, air entrapment during mixing or the arrangement of particles.

This very open and interconnected pore structure allows heat and mass transfer as well as moisture storage inside maize and sunflower concretes. The results underline the dependency of the hygrothermal and mechanical properties of vegetal concrete on the nature of both the bio-aggregates and the binder matrix. Thus, metakaolin-based materials have demonstrated better water vapour storage and permeability performances than LS composite and the use of pozzolanic binder matrix is favoured. Finally, even though all composites have proved to be excellent hygric regulators and good thermal insulators, the inhibitory effect of maize water-soluble components on concrete setting-time and mechanical behaviour does not allow MM concrete to be used. Hence, metakaolin and sunflower bark chips appear to be the most promising combination of raw materials for designing a hygrothermally and mechanically effective bio-aggregate based concrete. Hence, investigating the definition of a process to evaluate the overall potential and performances of bio-aggregates incorporated in a plant concrete could be an interesting prospect.

5 REFERENCES

ADEME (2018). Qui consomme le plus d'énergie en France ? (ADEME).

Amziane, S., and Arnaud, L. (2013). Bio-aggregate-based Building Materials: Applications to Hemp Concretes.

Amziane, S., and Collet, F. (2017). Bio-aggregates Based Building Materials (Dordrecht: Springer Netherlands).

Amziane, S., Collet, F., Lawrence, M., Magniont, C., Picandet, V., and Sonebi, M. (2017). Recommendation of the RILEM TC 236-BBM: characterisation testing of hemp shiv to determine the initial water content, water absorption, dry density, particle size distribution and thermal conductivity. Mater. Struct. *50*.

Arandigoyen, M., and Alvarez, J.I. (2006). Blended pastes of cement and lime: Pore structure and capillary porosity. Appl. Surf. Sci. *252*, 8077–8085.

Arandigoyen, M., Bernal, J.L.P., López, M.A.B., and Alvarez, J.I. (2005). Lime-pastes with different kneading water: Pore structure and capillary porosity. Appl. Surf. Sci. *252*, 1449–1459.

Arliguie, G., and Hornain, H. (2007). GranDuBé - Grandeurs associées à la durabilité des Bétons. Press. Lécole Natl. Ponts Chaussées.

Arnaud, L., and Gourlay, E. (2012). Experimental study of parameters influencing mechanical properties of hemp concretes. Constr. Build. Mater. *28*, 50–56.

Banhart, J. (2008). Advanced tomographic methods in materials research and engineering (Oxford ; New York: Oxford University Press).

Bouasker, M., Belayachi, N., Hoxha, D., and Al-Mukhtar, M. (2014). Physical Characterization of Natural Straw Fibers as Aggregates for Construction Materials Applications. Materials *7*, 3034–3048.

Bourdot, A., Moussa, T., Gacoin, A., Maalouf, C., Vazquez, P., Thomachot-Schneider, C., Bliard, C., Merabtine, A., Lachi, M., Douzane, O., et al. (2017). Characterization of a hemp-based agro-material: Influence of starch ratio and hemp shive size on physical, mechanical, and hygrothermal properties. Energy Build. *153*, 501–512.

Bourdot, A., Magniont, C., Lagouin, M., Lambaré, G., Labonne, L., and Evon, P. (2018). Evaluation of the potential of alternative particles as bio-aggregates for lightweight concrete. 7.

Brouard, Y., Belayachi, N., Hoxha, D., Ranganathan, N., and Méo, S. (2018). Mechanical and hygrothermal behavior of clay – Sunflower (Helianthus annuus) and rape straw (Brassica napus) plaster bio-composites for building insulation. Constr. Build. Mater. *161*, 196–207.

de Bruijn, P., and Johansson, P. (2013). Moisture fixation and thermal properties of lime–hemp concrete. Constr. Build. Mater. *47*, 1235–1242.

Cérézo, V. (2005). Propriétés mécaniques, thermiques et acoustiques d'un matériau à base de particules végétales: approche expérimentale et modélisation théorique.

Černý, R., Kunca, A., Tydlitát, V., Drchalová, J., and Rovnaníková, P. (2006). Effect of pozzolanic admixtures on mechanical, thermal and hygric properties of lime plasters. Constr. Build. Mater. *20*, 849–857.

Chabriac, P.A., Gourdon, E., Gle, P., Fabbri, A., and Lenormand, H. (2016). Agricultural by-products for building insulation: Acoustical characterization and modeling to predict micro-structural parameters. Constr. Build. Mater. *112*, 158–167.

Chamoin, J. (2013). Optimisation des propriétés (physiques, mécaniques et hydriques) de bétons de chanvre par la maîtrise de la formulation. INSA de Rennes.

Collet, F., and Pretot, S. (2012). Experimental investigation of moisture buffering capacity of sprayed hemp concrete. Constr. Build. Mater. *36*, 58–65.

Collet, F., and Pretot, S. (2014). Thermal conductivity of hemp concretes: Variation with formulation, density and water content. Constr. Build. Mater. *65*, 612–619.

Collet, F., Bart, M., Serres, L., and Miriel, J. (2008). Porous structure and water vapour sorption of hemp-based materials. Constr. Build. Mater. *22*, 1271–1280.

Collet, F., Chamoin, J., Pretot, S., and Lanos, C. (2013). Comparison of the hygric behaviour of three hemp concretes. Energy Build. *62*, 294–303.

Day, K.W., Aldred, J., and Hudson, B. (2013). Concrete mix design, quality control and specification (CRC Press).

Dinh, T.M. (2014). Contribution au développement de béton de chanvre préfabriqué utilisant un liant pouzzolanique innovant.

Dinh, T.M., Magniont, C., Coutand, M., and Escadeillas, G. (2012). Hemp concrete using innovative pozzolanic binder. p.

Diquélou, Y., Gourlay, E., Arnaud, L., and Kurek, B. (2015). Impact of hemp shiv on cement setting and hardening: Influence of the extracted components from the aggregates and study of the interfaces with the inorganic matrix. Cem. Concr. Compos. *55*, 112–121.

Driss, S. Analyse physique et caractérisation hygrothermique des matériaux de construction : approche expérimentale et modélisation numérique. 285.

Dubois, S. (2014). Modelling the hygrothermal behaviour of crop-based construction materials.

Elfordy, S., Lucas, F., Tancret, F., Scudeller, Y., and Goudet, L. (2008). Mechanical and thermal properties of lime and hemp concrete (“hempcrete”) manufactured by a projection process. Constr. Build. Mater. *22*, 2116–2123.

European Commission (2018). Buildings - Energy.

Evrard, A. (2006). Sorption behaviour of Lime-Hemp Concrete and its relation to indoor comfort and energy demand. 5.

Evrard, A. (2008). Transient hygrothermal behaviour of Lime-Hemp Materials. 142.

Feng, C., and Janssen, H. (2016). Hygric properties of porous building materials (II): Analysis of temperature influence. Build. Environ. *99*, 107–118.

Ghewy, X. (2017). Bilan 2014 de la production de déchets en France (MEEM).

Glé, P., Gourdon, E., and Arnaud, L. (2011). Acoustical properties of materials made of vegetable particles with several scales of porosity. Appl. Acoust. *72*, 249–259.

GNIS Groupement National Interprofessionnel des Semences et plants.

Gourlay, E., Glé, P., Marceau, S., Foy, C., and Moscardelli, S. (2017). Effect of water content on the acoustical and thermal properties of hemp concretes. Constr. Build. Mater. *139*, 513–523.

Hustache, Y., and Arnaud, L. (2008). Synthèse des connaissances sur les bétons et mortiers de chanvre.

InterChanvre (2017). Plan Filière de l'interprofession du chanvre (InterChanvre).

Jiang, Y., Ansell, M., Jia, X., Hussain, A., and Lawrence, M. (2017). Physical characterisation of hemp shiv: Cell wall structure and porosity. p.

Jiang, Y., Lawrence, M., Ansell, M.P., and Hussain, A. (2018). Cell wall microstructure, pore size distribution and absolute density of hemp shiv. R. Soc. Open Sci. *5*, 171945.

Labat, M., Magniont, C., Oudhof, N., and Aubert, J.-E. (2016). From the experimental characterization of the hygrothermal properties of straw-clay mixtures to the numerical assessment of their buffering potential. Build. Environ. *97*, 69–81.

Laborel-Préneron, A. (2017). Formulation and characterization of unfired clay bricks with plant aggregates.pdf. Université de Toulouse, Université Toulouse III-Paul Sabatier.

Laborel-Préneron, A., Magniont, C., and Aubert, J.-E. (2017). Characterization of Barley Straw, Hemp Shiv and Corn Cob as Resources for Bioaggregate Based Building Materials. Waste Biomass Valorization.

Latif, E., Ciupala, M.A., Tucker, S., Wijeyesekera, D.C., and Newport, D.J. (2015). Hygrothermal performance of wood-hemp insulation in timber frame wall panels with and without a vapour barrier. Build. Environ. *92*, 122–134.

Lawrence, M., Fodde, E., Paine, K., and Walker, P. (2012). Hygrothermal performance of an experimental hemp-lime building. In Key Engineering Materials, (Trans Tech Publ), pp. 413–421.

Lenormand, H., Mahieu, A., Leblanc, N., and Vivet, A. (2014). Nouvelles agroressources pour panneaux de particules 100% biosourcés. 11.

Magniont, C. (2010). Contribution à la formulation et à la caractérisation d'un écomatériau de construction à base d'agroressources. Université de Toulouse, Université Toulouse III-Paul Sabatier.

Mazhoud, B., Collet, F., Pretot, S., and Lanos, C. (2017). Mechanical properties of hemp-clay and hemp stabilized clay composites. Constr. Build. Mater. *155*, 1126–1137.

Merle, J., Sénéchal, P., Guerton, F., Moonen, P., Trinsoutrot, P., Birot, M., and Charrier-El Bouhtoury, F. (2016). Microstructural characterization of biobased carbon foam by means of X-ray microtomography and compared to conventional techniques. RSC Adv. *6*, 96057–96064.

Moujalled, B., Aït Ouméziane, Y., Moissette, S., Bart, M., Lanos, C., and Samri, D. (2018). Experimental and numerical evaluation of the hygrothermal performance of a hemp lime concrete building: A long term case study. Build. Environ. *136*, 11–27.

Murphy, F., Pavia, S., and Walker, P. (2010). An assessment of the physical properties of lime-hemp concrete. (Cork: Ní Nualláin, Walsh, West, Cannon, Caprani, McCabe), p.

Nežerka, V., Slížková, Z., Tesárek, P., Plachý, T., Frankeová, D., and Petráňová, V. (2014). Comprehensive study on mechanical properties of lime-based pastes with additions of metakaolin and brick dust. Cem. Concr. Res. *64*, 17–29.

Nguyen, T.T. (2010). Contribution à l'étude de la formulation et du procédé de fabrication d'éléments de construction en béton de chanvre. PhD Thesis. Université de Bretagne Sud.

Nguyen, T.T., Picandet, V., Carre, P., Lecompte, T., Amziane, S., and Baley, C. (2010). Effect of compaction on mechanical and thermal properties of hemp concrete. Eur. J. Environ. Civ. Eng. *14*, 545–560.

Niyigena, C., Amziane, S., Chateauneuf, A., Arnaud, L., Bessette, L., Collet, F., Lanos, C., Escadeillas, G., Lawrence, M., Magniont, C., et al. (2016). Variability of the mechanical properties of hemp concrete. Mater. Today Commun. *7*, 122–133.

Niyigena, C., Amziane, S., and Chateauneuf, A. (2018). Multicriteria analysis demonstrating the impact of shiv on the properties of hemp concrete. Constr. Build. Mater. *160*, 211–222.

Nozahic, V. (2012). Vers une nouvelle démarche de conception des bétons de végétaux lignocellulosiques basée sur la compréhension et l'amélioration de l'interface liant/végétal: application à des granulats de chenevotte et de tige de tournesol associés à un liant ponce/chaux. Université Blaise Pascal-Clermont-Ferrand II.

Nunes, C., Slížková, Z., Stefanidou, M., and Němeček, J. (2016). Microstructure of lime and lime-pozzolana pastes with nanosilica. Cem. Concr. Res. *83*, 152–163.

Palumbo, M., Lacasta, A.M., Holcroft, N., Shea, A., and Walker, P. (2016). Determination of hygrothermal parameters of experimental and commercial bio-based insulation materials. Constr. Build. Mater. *124*, 269–275.

Peñaloza, D., Erlandsson, M., and Falk, A. (2016). Exploring the climate impact effects of increased use of bio-based materials in buildings. Constr. Build. Mater. *125*, 219–226.

Rahim, M., Douzane, O., Tran Le, A.D., Promis, G., Laidoudi, B., Crigny, A., Dupre, B., and Langlet, T. (2015). Characterization of flax lime and hemp lime concretes: Hygric properties and moisture buffer capacity. Energy Build. *88*, 91–99.

Rahim, M., Douzane, O., Tran Le, A.D., Promis, G., and Langlet, T. (2016). Characterization and comparison of hygric properties of rape straw concrete and hemp concrete. Constr. Build. Mater. *102*, 679–687.

Ratiarisoa, R.V., Magniont, C., Ginestet, S., Oms, C., and Escadeillas, G. (2016). Assessment of distilled lavender stalks as bioaggregate for building materials: Hygrothermal properties, mechanical performance and chemical interactions with mineral pozzolanic binder. Constr. Build. Mater. *124*, 801–815.

Rode, C., Peuhkuri, R.H., Mortensen, L.H., Hansen, K.K., Time, B., Gustavsen, A., Ojanen, T., Ahonen, J., Svennberg, K., and Arfvidsson, J. (2005). Moisture buffering of building materials.

Samri, D. (2008). Analyse physique et caractérisation hygrothermique des matériaux de construction : approche expérimentale et modélisation numérique.

Sidi Mohamed, A., Sabathier, V., Evon, P., Magniont, C., and Labonne, L. (2017). Contribution to the design and the characterization of a fully bio-based insulated panel including sunflower pith (Clermont-Ferrand, France).

Sing, K.S.W. (1985). Reporting physisorption data for gas/solid systems with special reference to the determination of surface area and porosity (Recommendations 1984). Pure Appl. Chem. *57*, 603–619.

SOeS (2016). La consommation intérieure de matières en France (Service de l'Observation et des Statistiques - Ministère de la transistion écologique et solidaire).

Stefanidou, M., Assael, M., Antoniadis, K., and Matziaroglou, G. (2010). Thermal Conductivity of Building Materials Employed in the Preservation of Traditional Structures. Int. J. Thermophys. *31*, 844–851.

Tracz, T. (2016). Open porosity of cement pastes and their gas permeability. Bull. Pol. Acad. Sci. Tech. Sci. *64*.

Tran Le, A.D. (2010). Etude des transferts hygrothermiques dans le béton de chanvre et leur application au bâtiment (sous titre: simulation numérique et approche expérimentale). 220.

Tran Le, A.D., Maalouf, C., Mai, T.H., Wurtz, E., and Collet, F. (2010). Transient hygrothermal behaviour of a hemp concrete building envelope. Energy Build. *42*, 1797–1806.

Viel, M., Collet, F., and Lanos, C. (2018). Chemical and multi-physical characterization of agro-resources' by-product as a possible raw building material. Ind. Crops Prod. *120*, 214–237.

Vololonirina, O., and Perrin, B. (2016). Inquiries into the measurement of vapour permeability of permeable materials. Constr. Build. Mater. *102*, 338–348.

Walker, R., and Pavía, S. (2014). Moisture transfer and thermal properties of hemp–lime concretes. Constr. Build. Mater. *64*, 270–276.

Walker, R., Pavia, S., and Mitchell, R. (2014). Mechanical properties and durability of hemp-lime concretes. Constr. Build. Mater. *61*, 340–348.

Williams, J., Lawrence, M., and Walker, P. (2016). A method for the assessment of the internal structure of bio-aggregate concretes. Constr. Build. Mater. *116*, 45–51.

Williams, J., Lawrence, M., and Walker, P. (2018). The influence of constituents on the properties of the bio-aggregate composite hemp-lime. Constr. Build. Mater. *159*, 9–17.